Suspensions and suspension mechanics

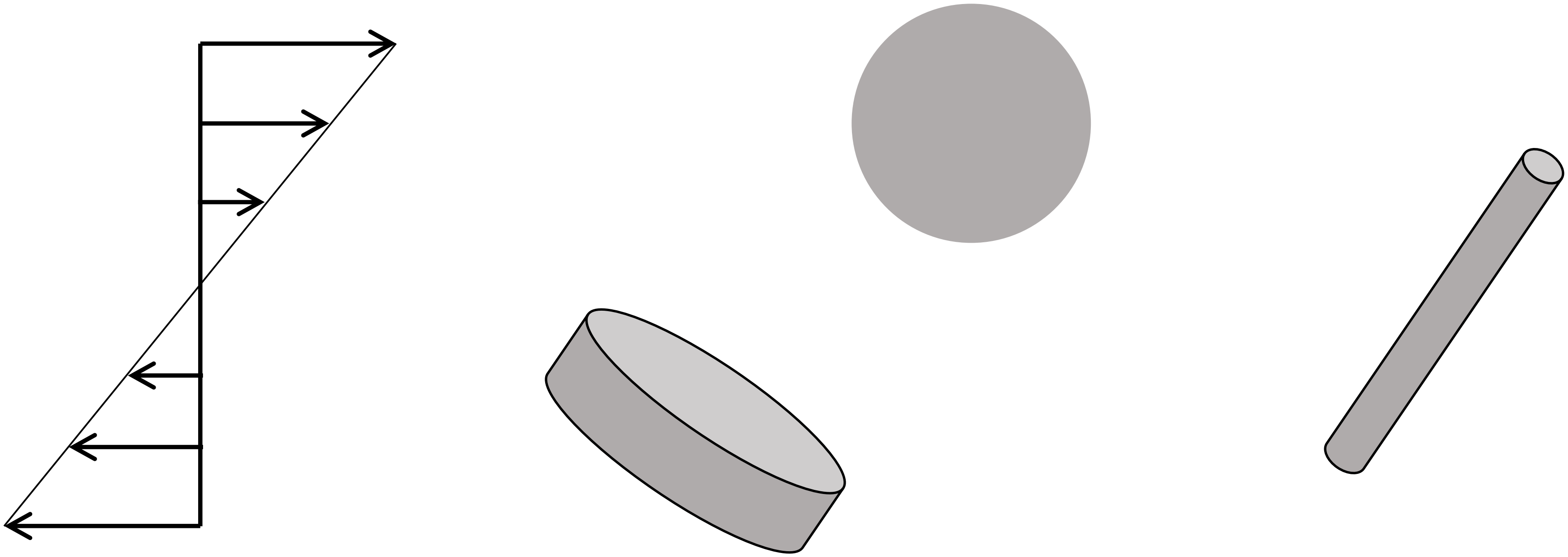

Suspensions may be distinguished by the shape and size of the discrete phase

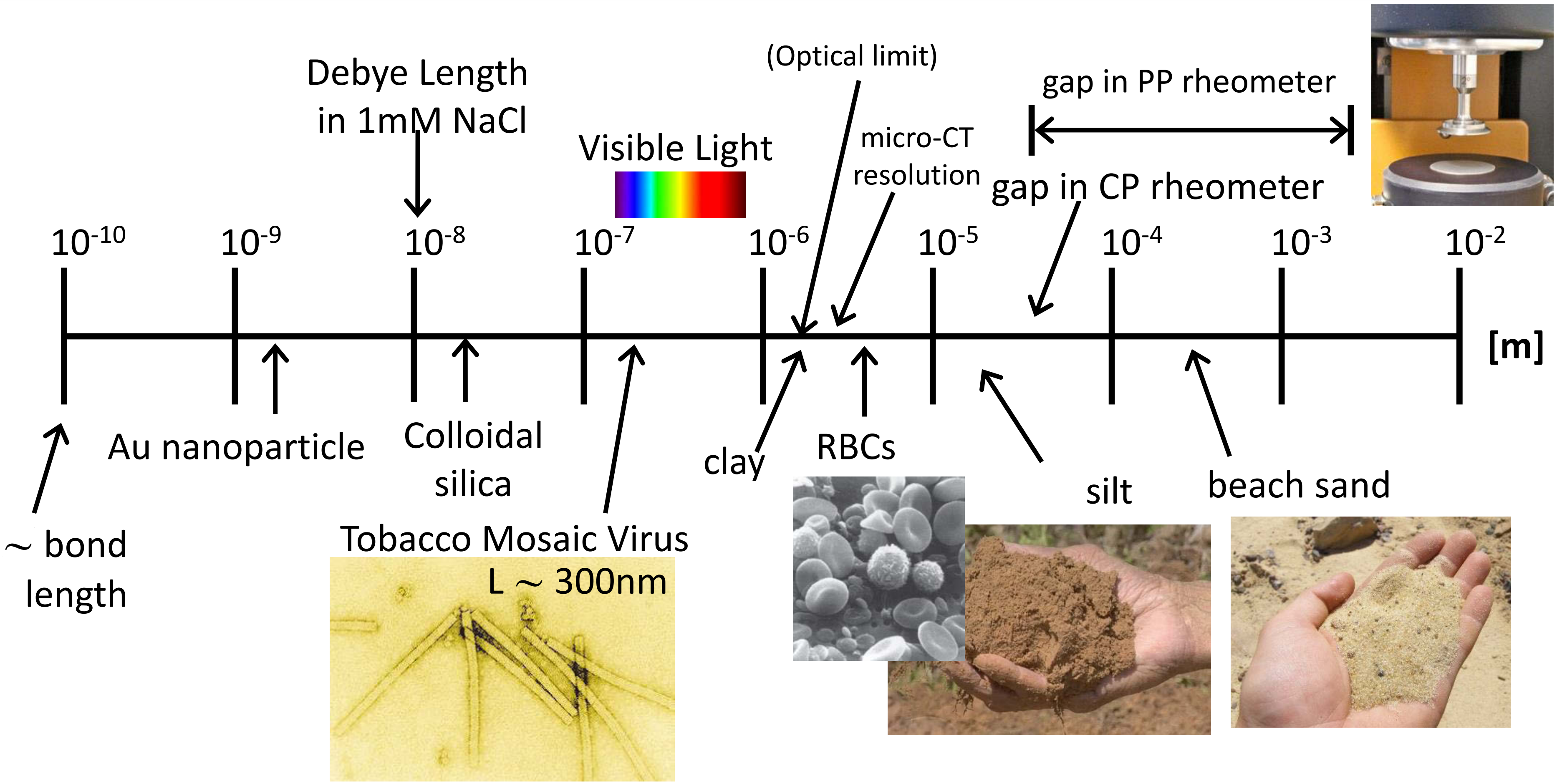

Size is important: indicates the relevance of various forces

Strong function of volume fraction

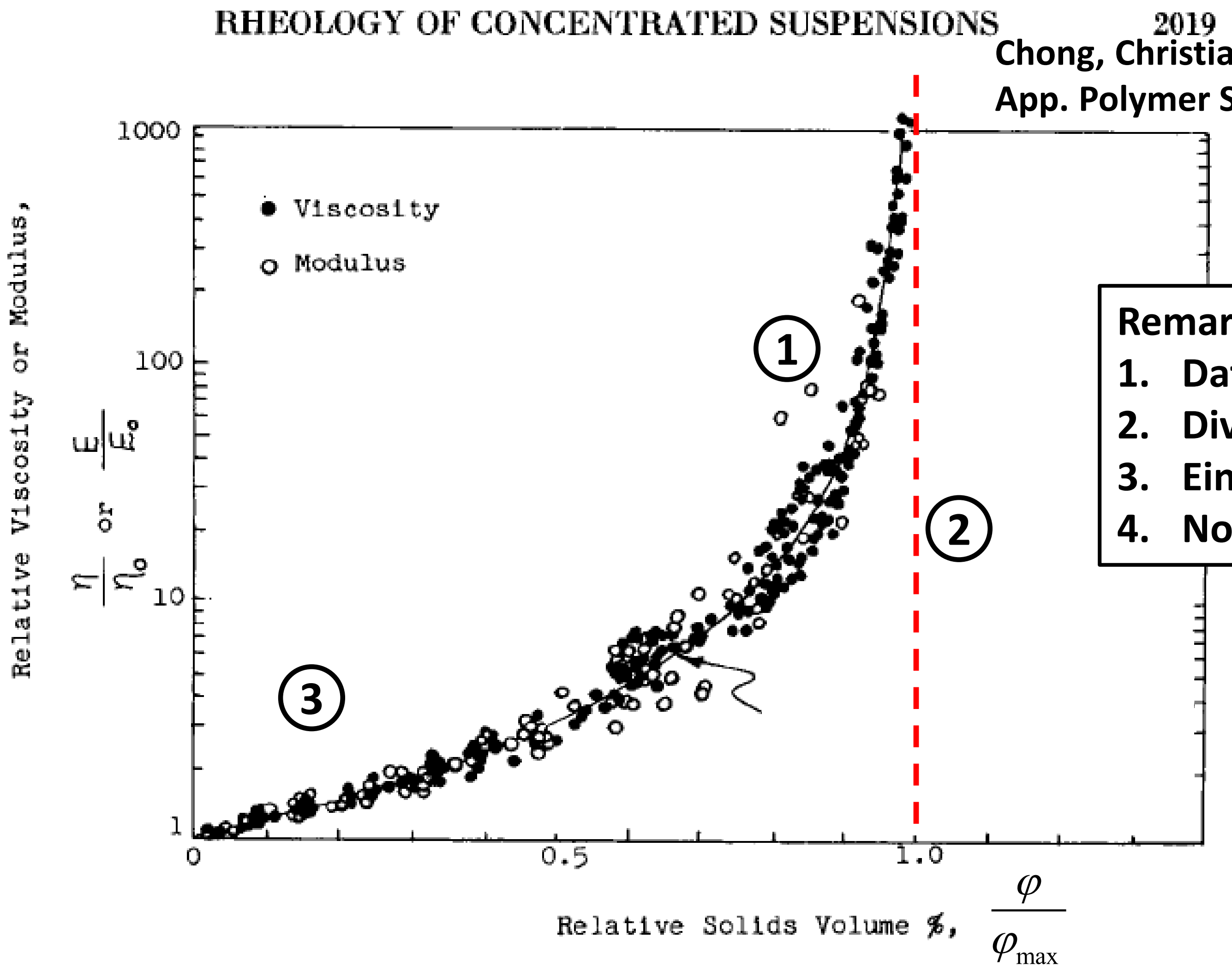

Chong, Christiansen, & Baer J. App. Polymer Sci. 1971

Remarks:

1. Data from 16 sources
2. Divergence at ϕ_{max}
3. Einstein limit at low ϕ
4. No rate dependence

Fig. 11. Dependence of relative viscosity or modulus on solids concentrations.

Strong function of volume fraction

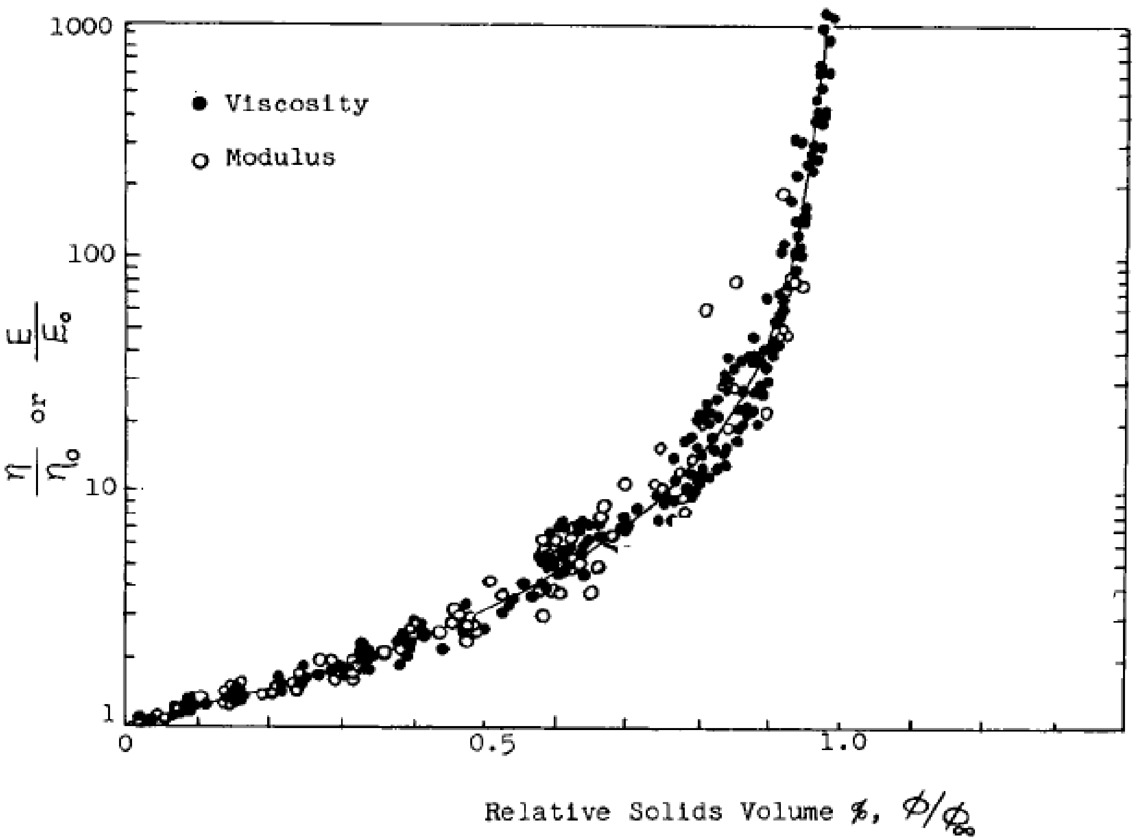

$$\eta_r = f(\varphi)$$

Entirety of rheology reduced to one variable.

Is this always the case?

Under what conditions is this valid?

Strong function of volume fraction, distribution of sizes

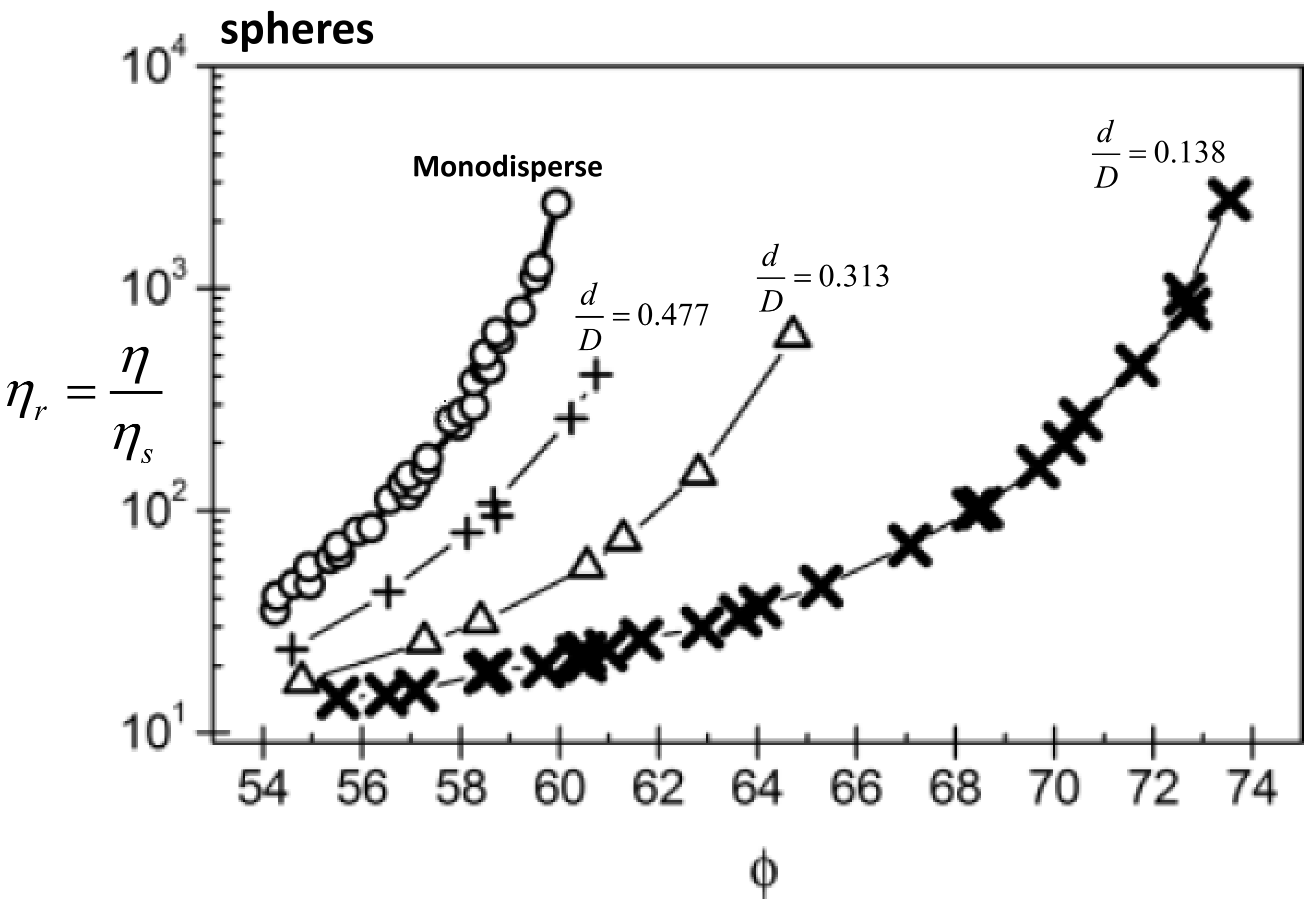

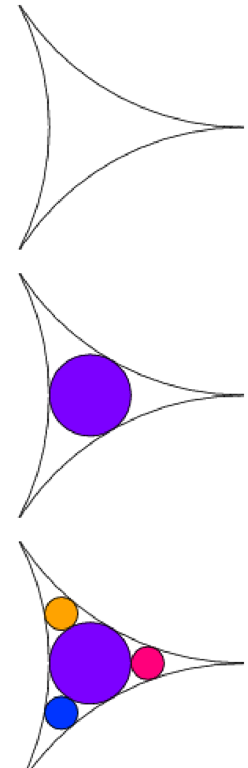

Chong, Christiansen, & Baer J. App. Polymer Sci. 1971 (adapted)

The Farris effect

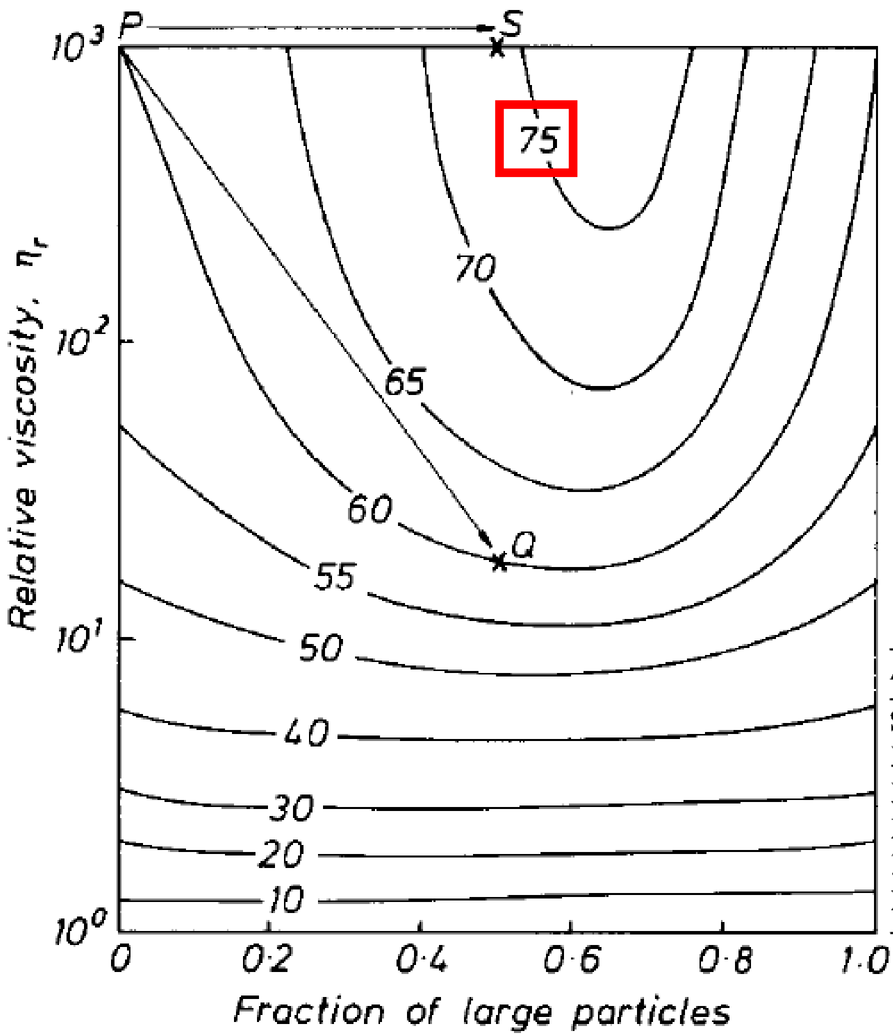

Contours: volume fraction

5:1 ratio in particle size

What are the paths P→S and P→Q?

Arrangement	Maximum packing fraction
Simple cubic	0.52
Minimum thermodynamically stable configuration	0.548
Hexagonally packed sheets just touching	0.605
Random close packing	0.637
Body-centred cubic packing	0.68
Face-centred cubic/ hexagonal close packed	0.74

<0.75

Particle shape is also important

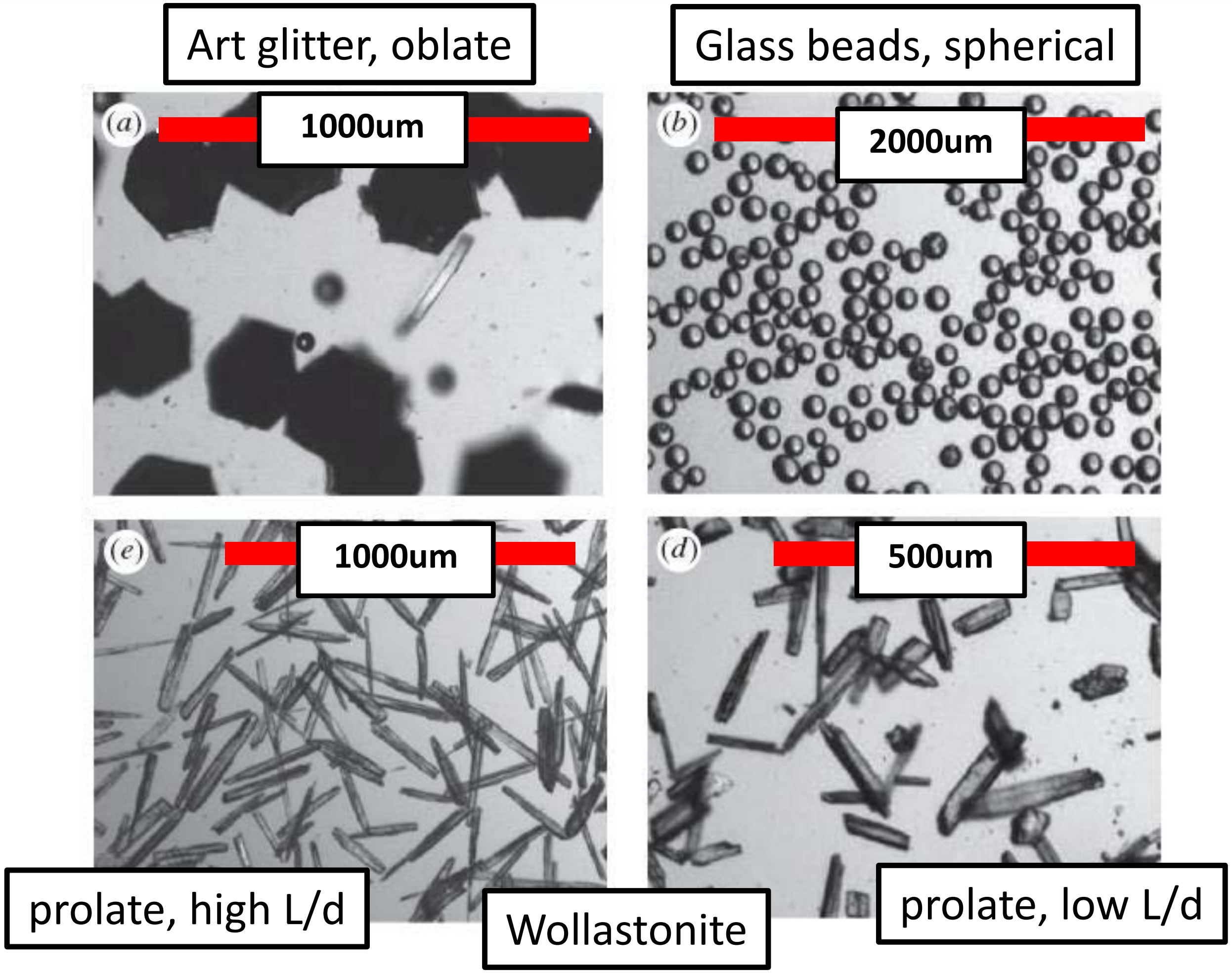

Mueller, S., et al. Proc. R. Soc. A (2010) 466:1201-1228

Elongated particles have greater hydrodynamic interactions

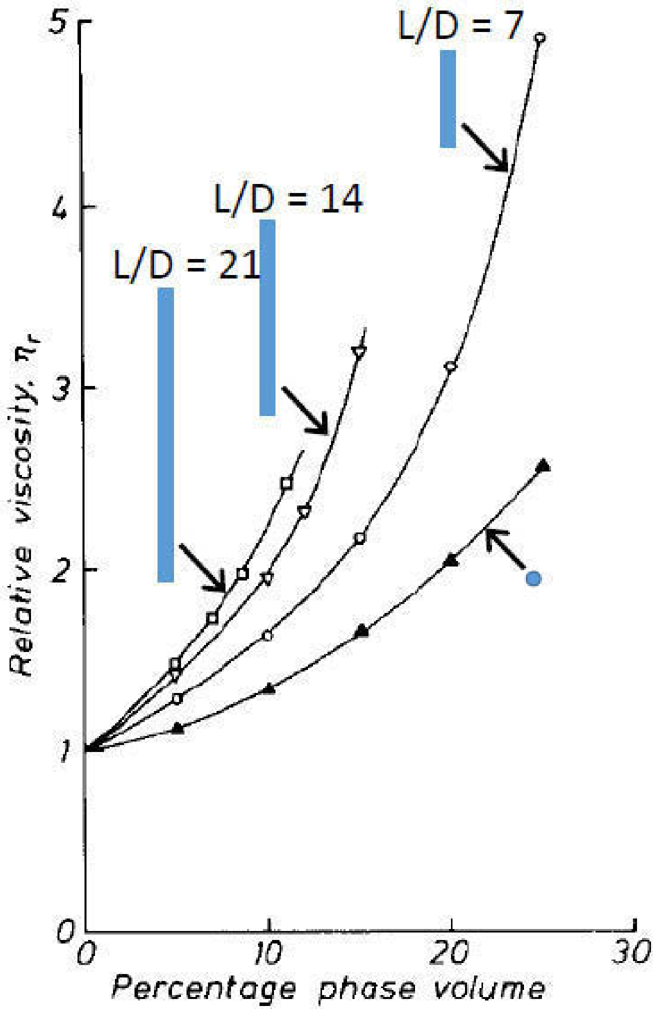

For the same volume fraction, greater thickening of suspensions when L/D becomes large.

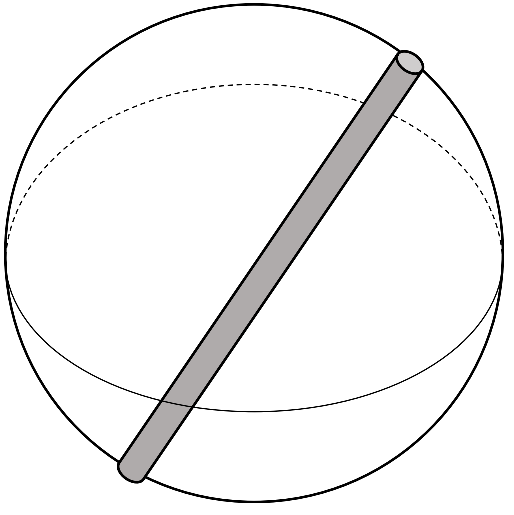

Particle rotates and sweeps out a volume

From Barnes, et al. “An Introduction to Rheology”

A sample-spanning structure occurs at low volume fractions

Garboczi, et al., Phys. Rev. E. (1995) 52:819-828

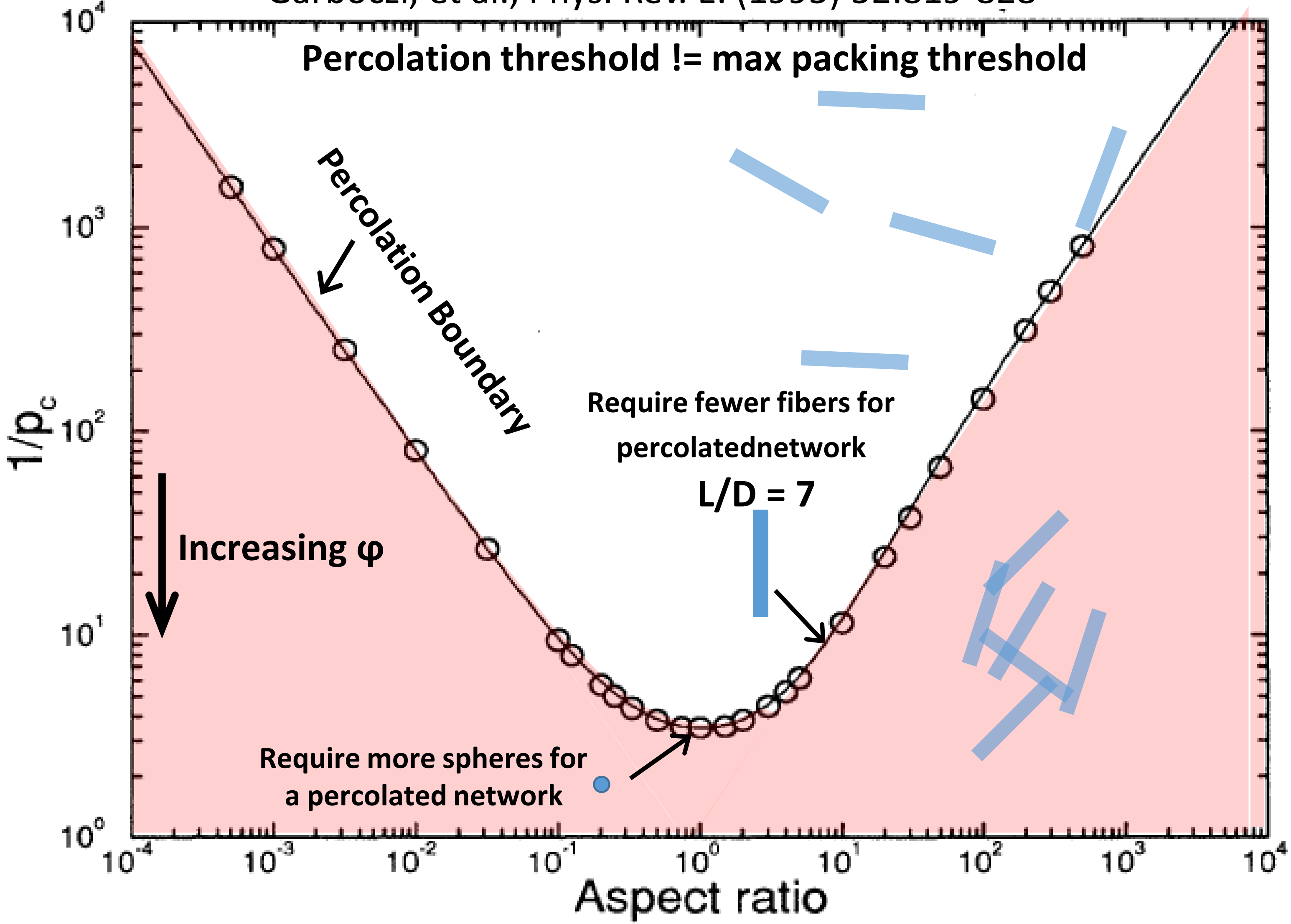

Despite this scaling, we still see a shear rate dependence at large Pe#

The characterization of the total stress of concentrated suspensions of noncolloidal spheres in Newtonian fluids

Isidro E. Zarraga, Davide A. Hill, and David T. Leighton, Jr.[a)]

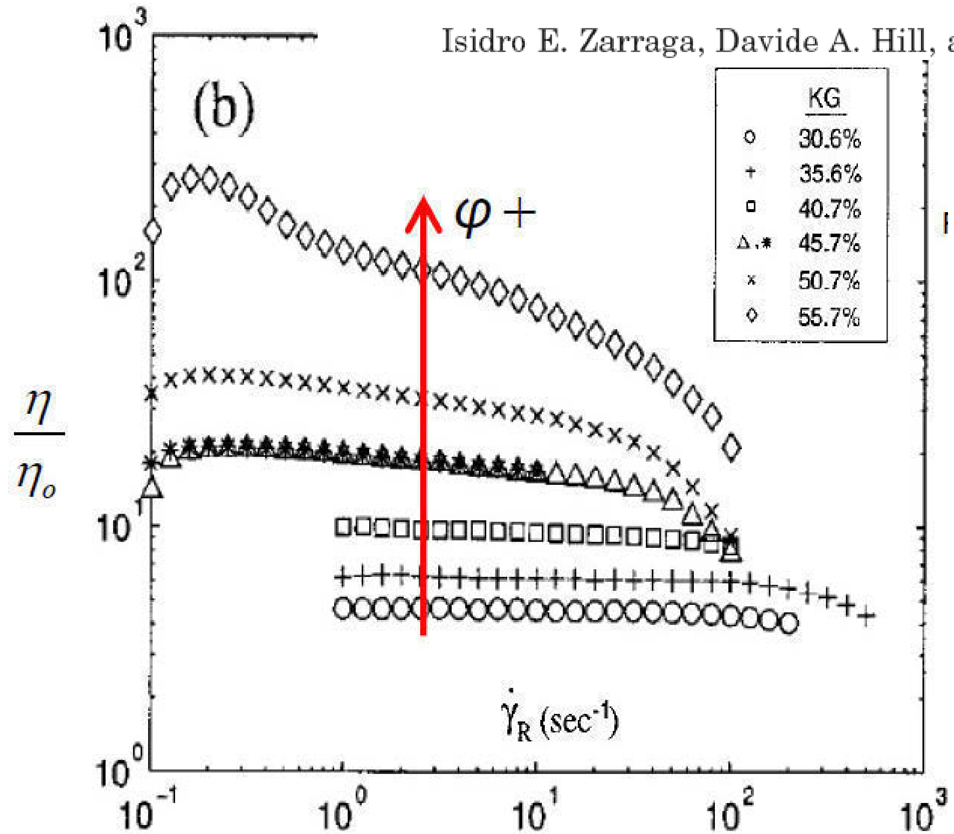

Remarks:

1. This is a non-colloidal suspension of spheres
2. Brownian diffusion is weak.
3. Shear thinning is observed (?)
4. How did we construct the earlier viscosity curves with no rate dependence?
5. Glass particles in a Newtonian matrix

Zarraga, Hill, and Leighton J. Rheol. 2000 (44)

Turn on Brownian motion, dependence on Pe

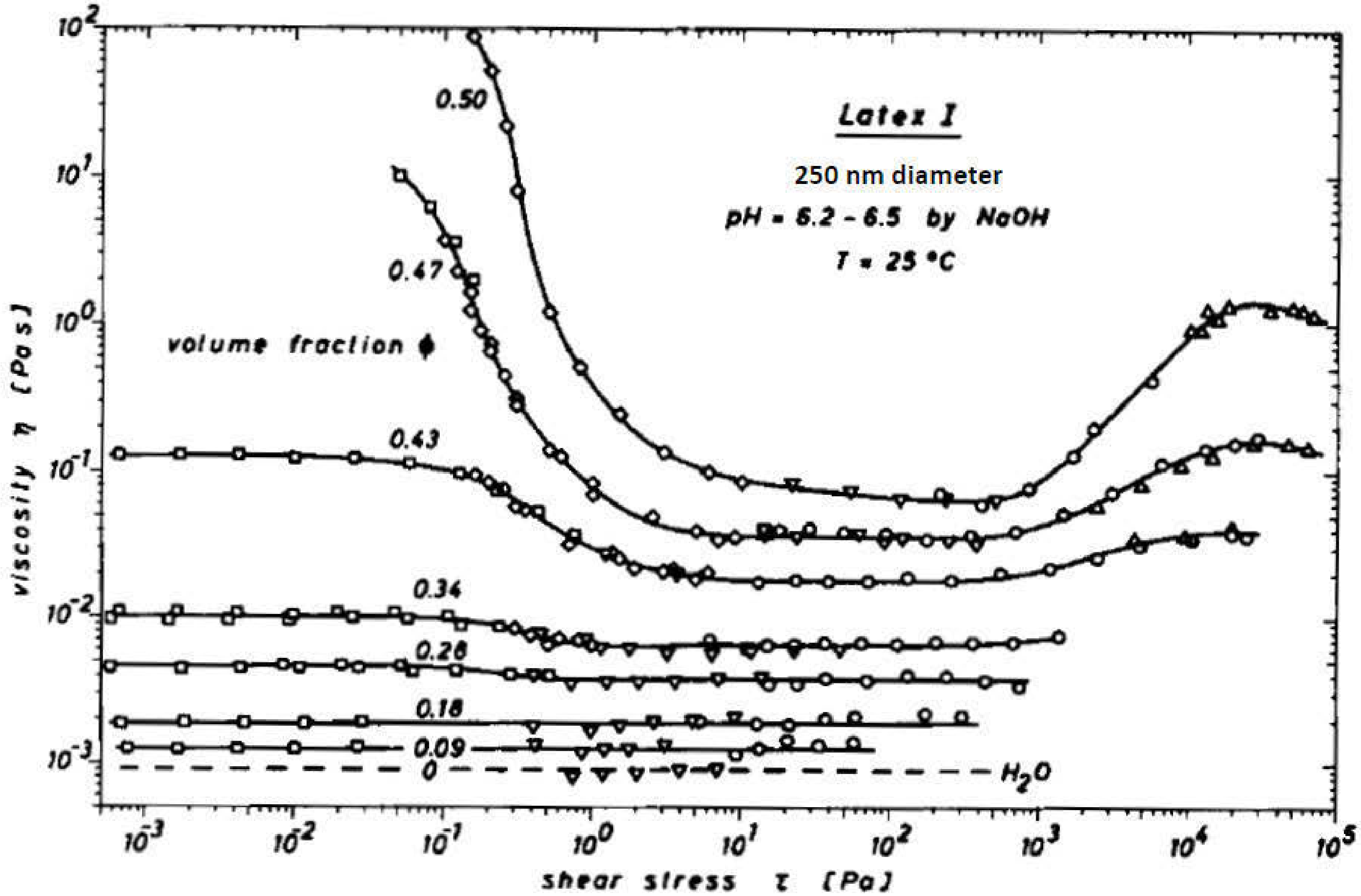

Laun, H. M. Angew. Makro. Chem. 1984, 124:335-359

Turn on Brownian motion, dependence on Pe

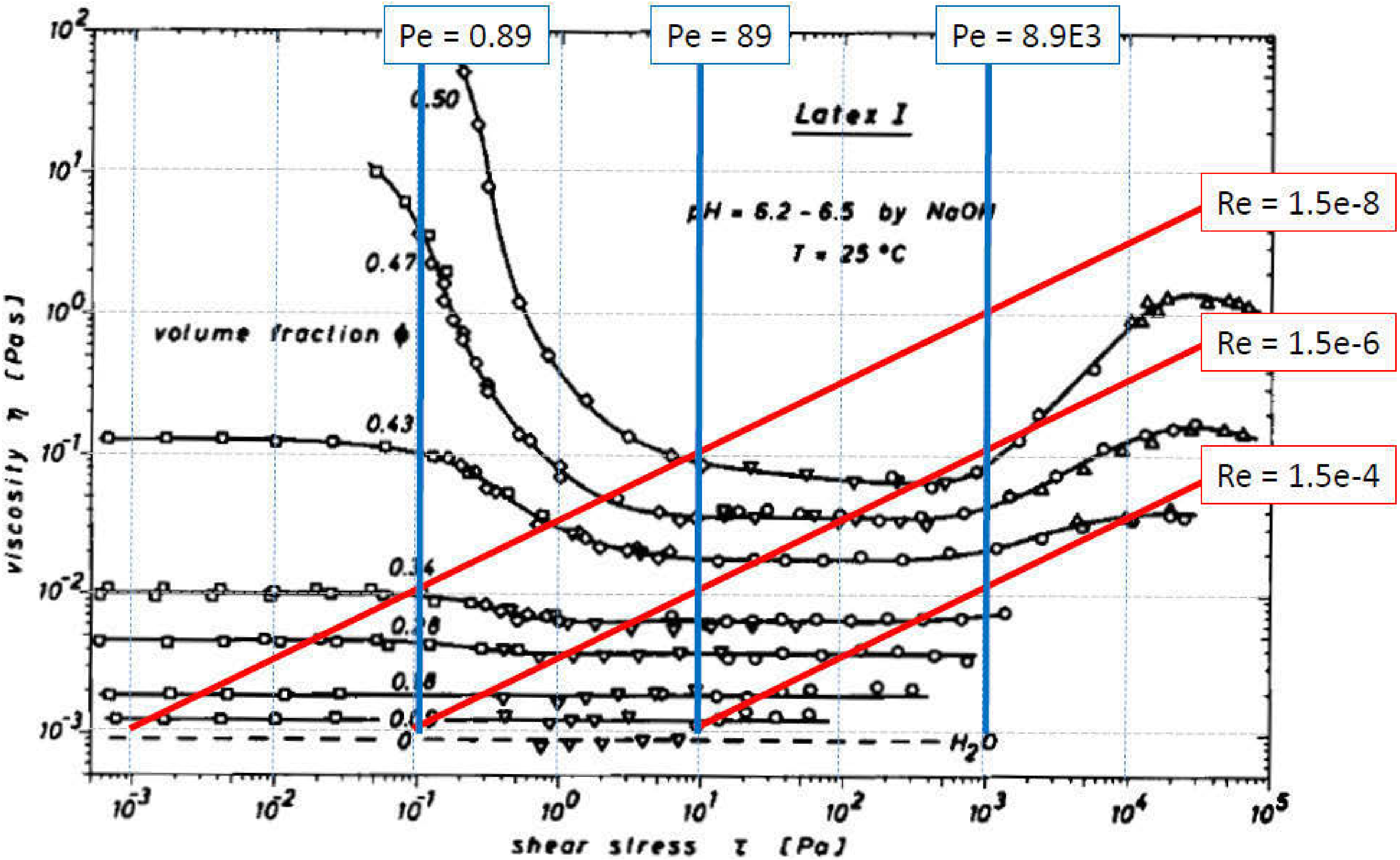

Laun, H. M. Angew. Makro. Chem. 1984, 124:335-359

Turn on Brownian motion, dependence on Pe

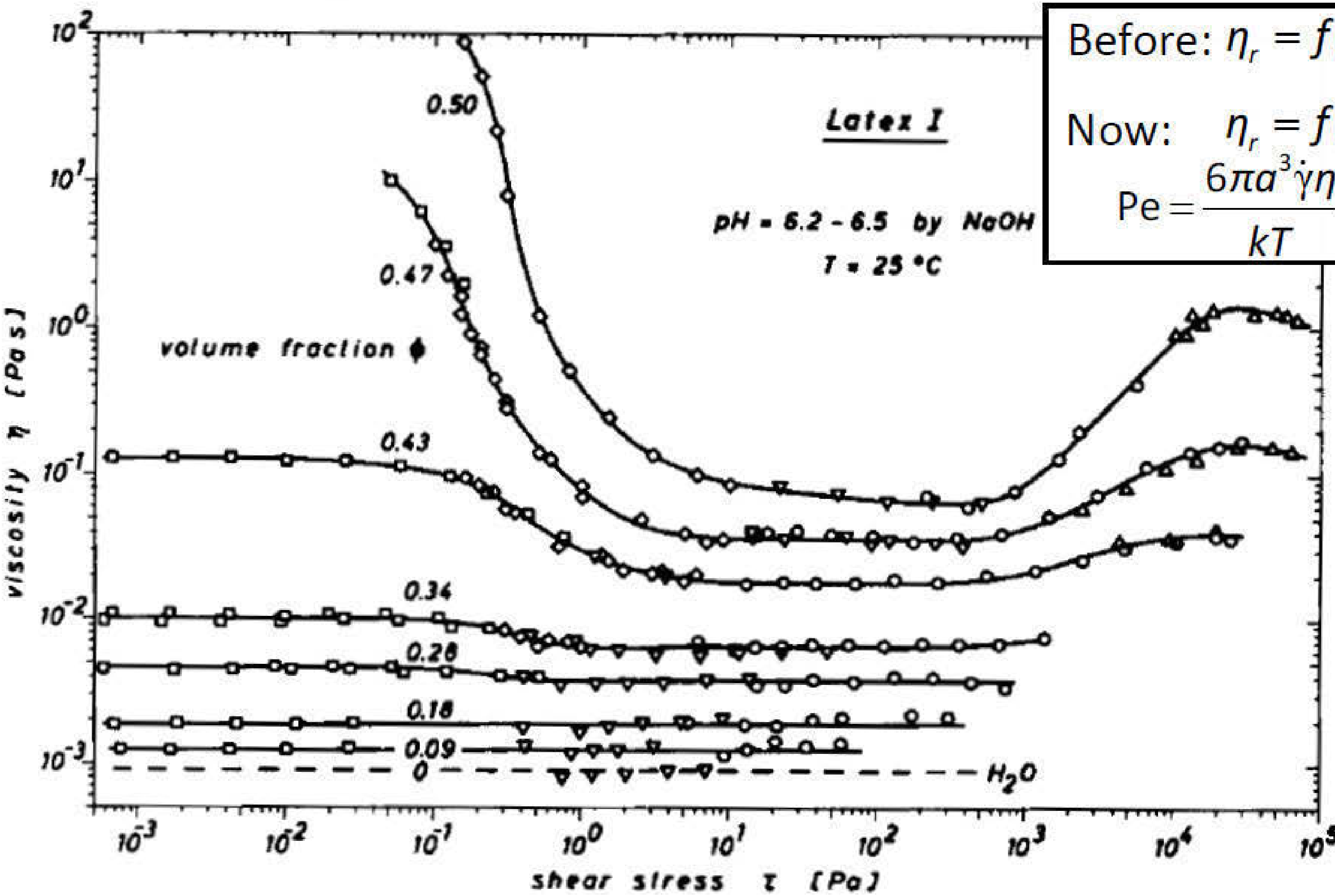

Before: $\eta_r = f(\varphi)$

Now: $\eta_r = f(\varphi, \mathrm{Pe})$

$$\mathrm{Pe} = \frac{6\pi a^3 \dot{\gamma} \eta}{kT}$$

Laun, H. M. Angew. Makro. Chem. 1984, 124:335-359

Limiting trajectories for particle–particle interactions

- Batchelor & Green result
  - C_2 accounts for pair interactions, depends on type of flow
  - Orbital capture problem, dependence on Pe

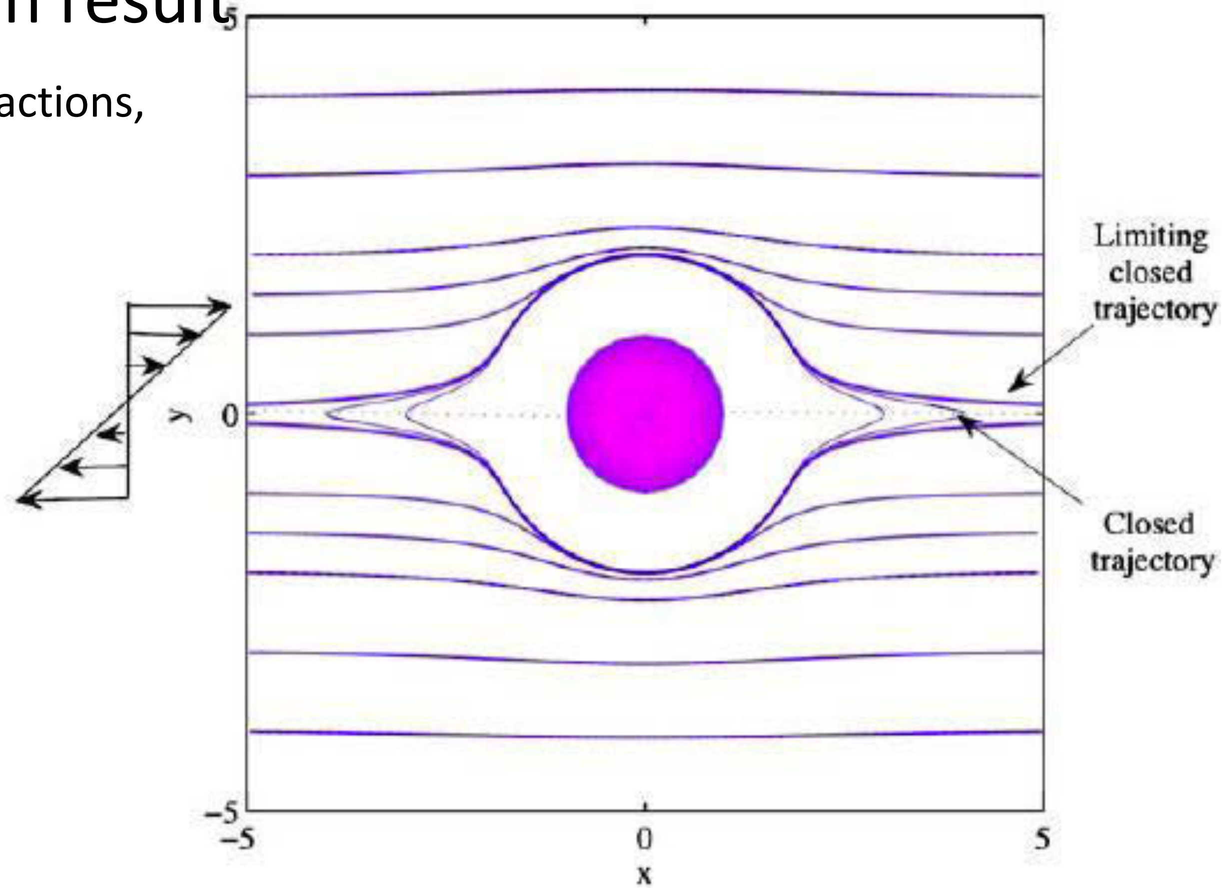

Morris, J. F. "A review of microstructure in concentrated suspensions and its implications for rheology and bulk flow" (2009) 48:909-923

Microstructure is the source of non-Newtonian properties

Microstructure in suspensions: position and orientation of particles

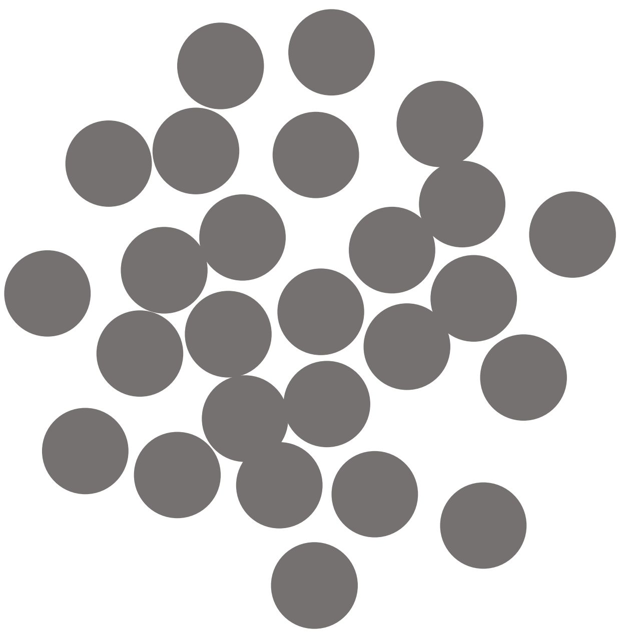

What is the local density around one particle?

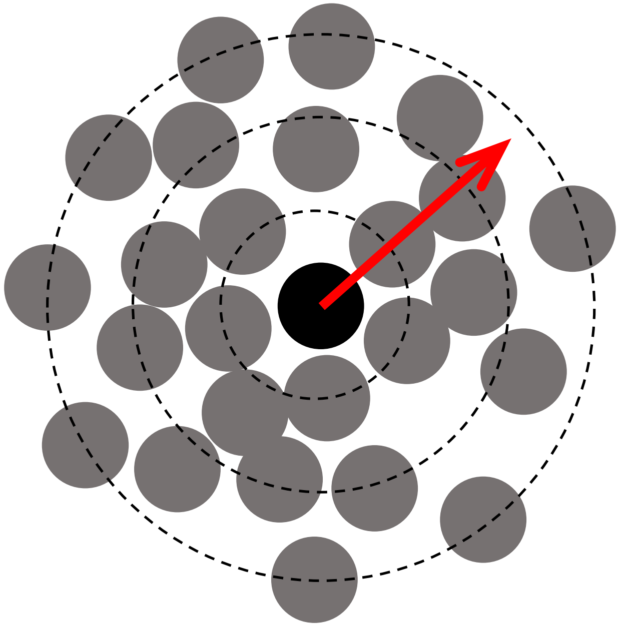

Count neighboring particles as a function of distance

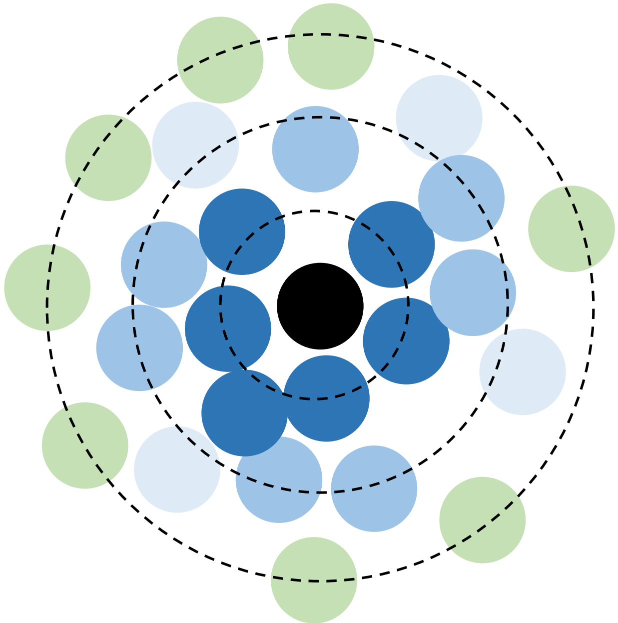

Find 1st, 2nd, 3rd, etc.. nearest neighbors

Radial symmetry is not guaranteed

In general, particle distribution is a function of an **angle** and **distance**

$$g(r,\theta) = \frac{\text{Local density}}{\text{Bulk density}}$$

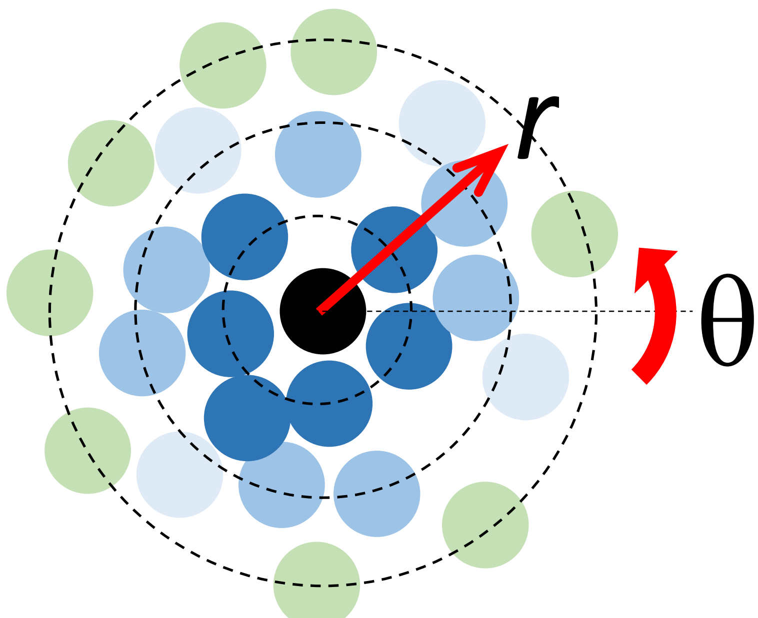

Investigate hydrodynamics to understand ordering by hydrodynamic forces

Experiments: Parsi & Gadala-Maria

High Pe # spheres

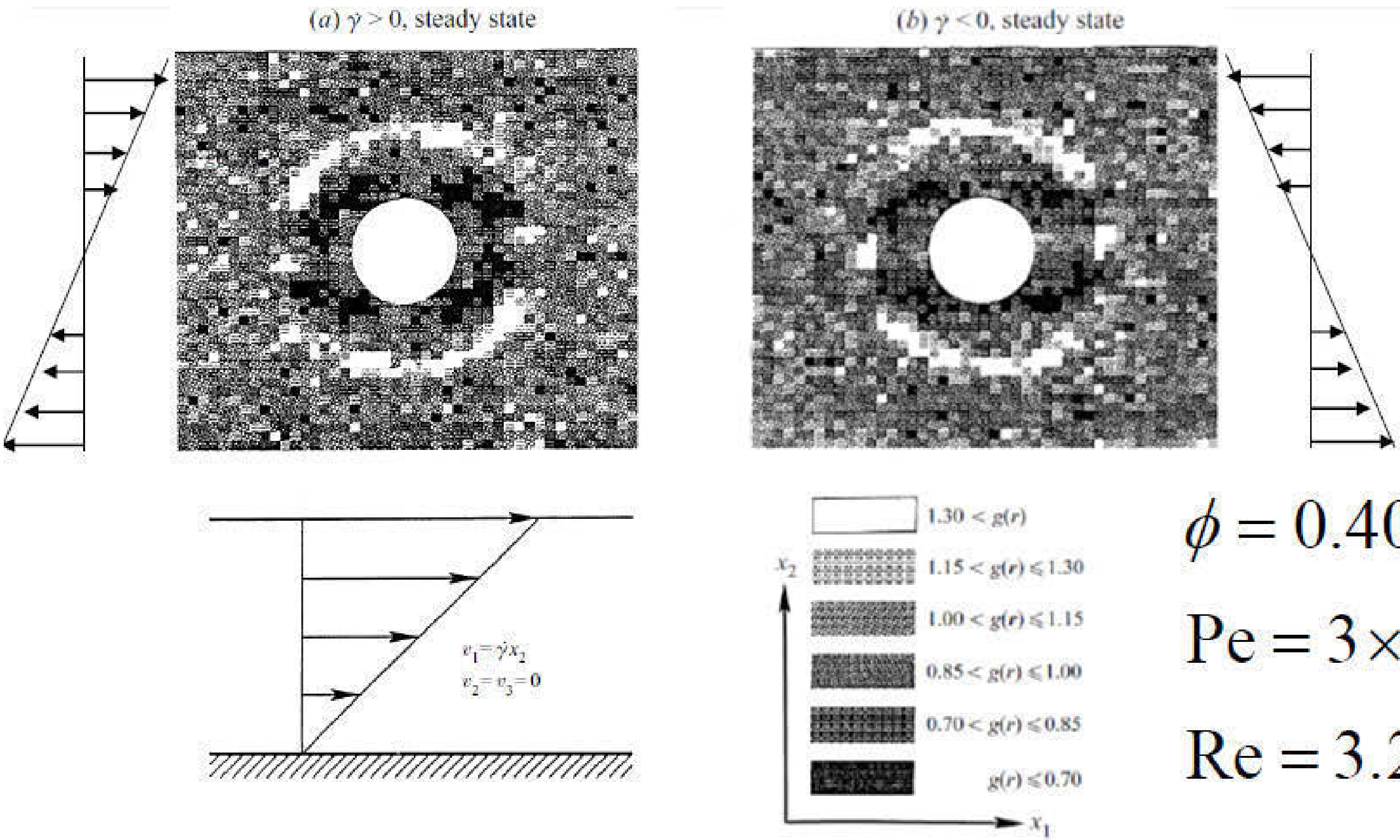

$$\phi = 0.40$$

$$\mathrm{Pe} = 3 \times 10^5$$

$$\mathrm{Re} = 3.2 \times 10^{-7}$$

FIGURE 2. Pair-distribution function g in the plane of shear for a suspension of polystyrene spheres in silicone oil at particle volume fraction $\phi = 0.4$ in simple shear at $Pe = 3.0 \times 10^5$ and $Re = 3.2 \times 10^{-7}$. The shear rate is opposite in the two plots. Note the fore-aft asymmetry of the pair distribution and the reversal of the asymmetry for reversal of the shear rate. From Parsi & Gadala-Maria (1987).

Simulations: Péclet number determines symmetry of distribution

Pe = 0, φ = .45

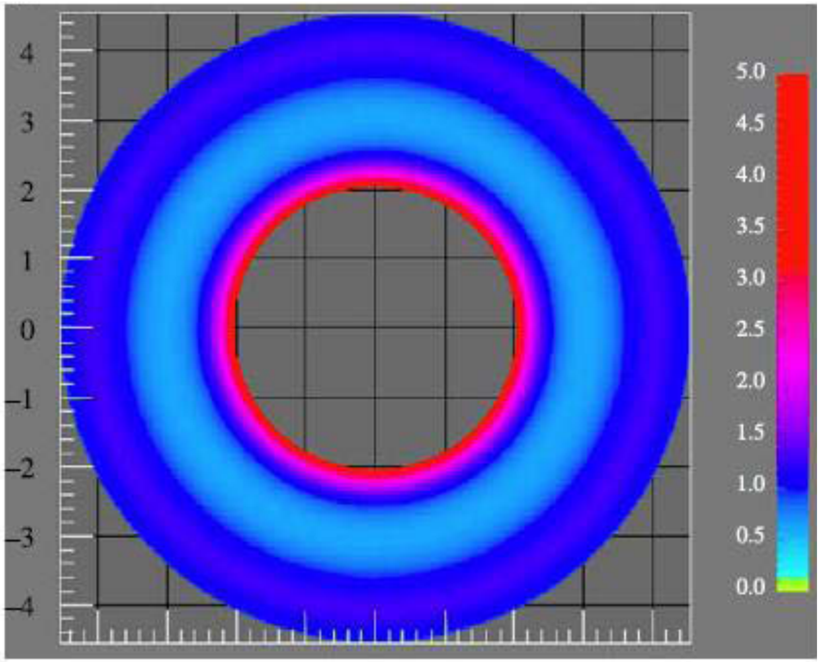

Pe = 25, φ = .3

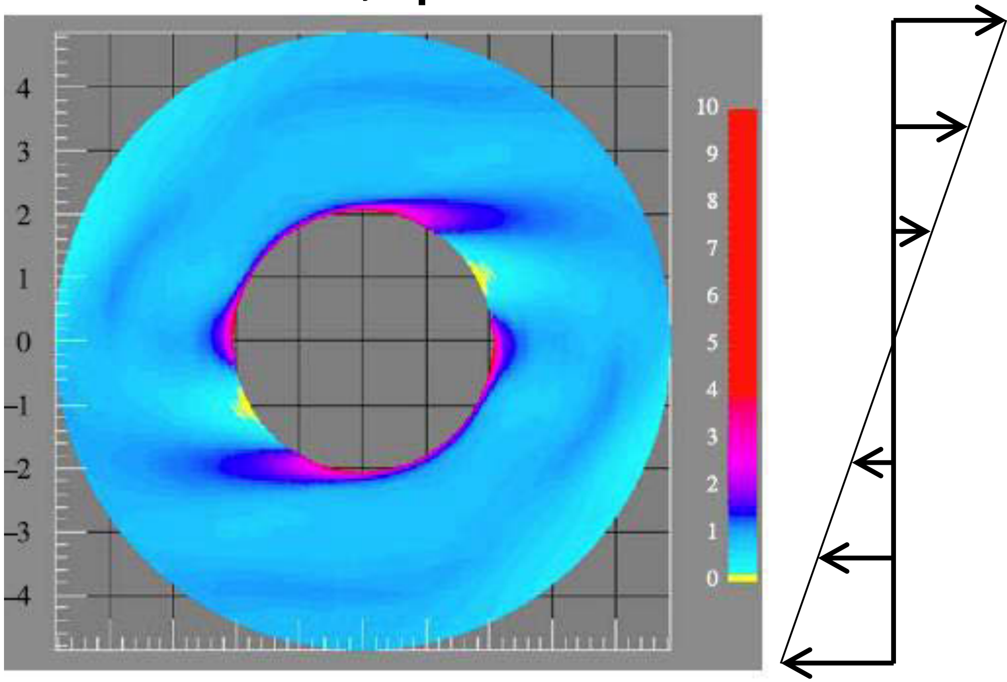

Color indicates density of particle centers

- At low Pe, randomized
- At higher Pe, induced structure from flow

Increased particle density along shoulders of particles, attempting to align in rows

Morris, J. F. "A review of microstructure in concentrated suspensions and its implications for rheology and bulk flow" (2009) 48:909-923

Simulations: Péclet number determines symmetry of distribution

Pe = 0, φ = .45

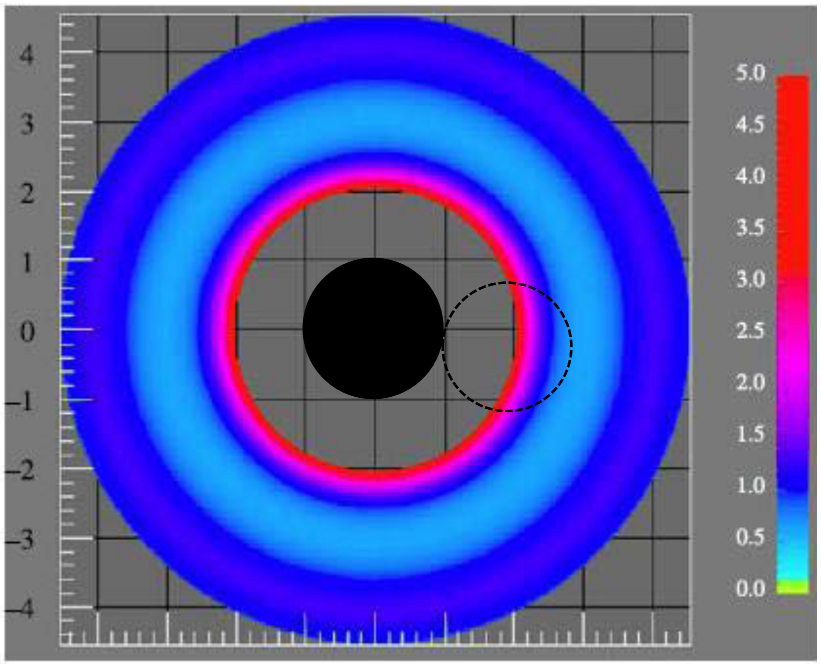

Pe = 25, φ = .3

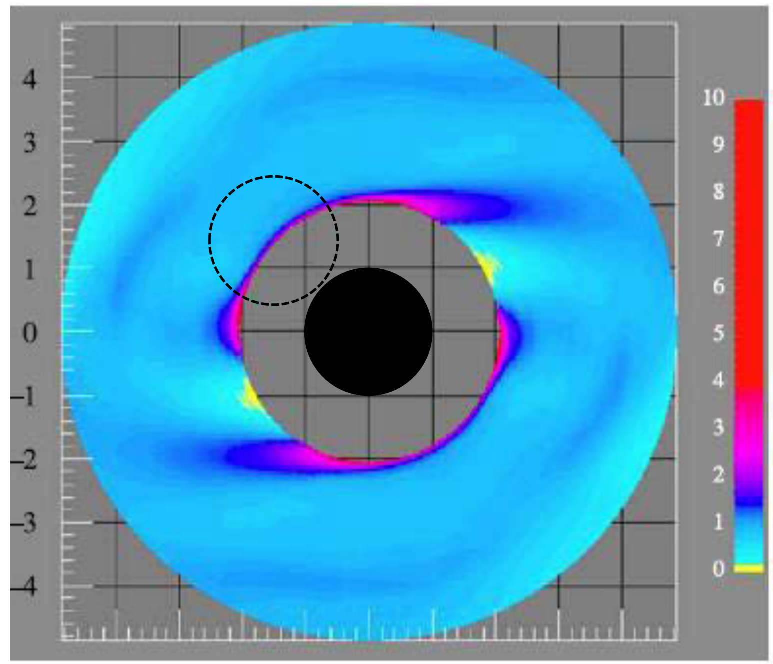

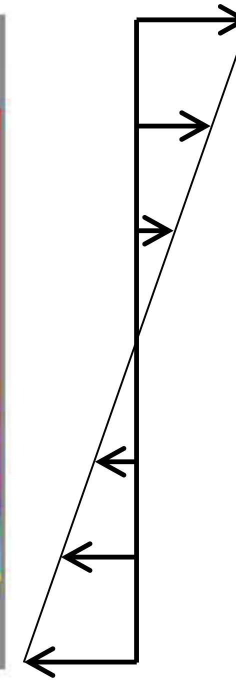

Color indicates density of particle centers

- At low Pe, randomized
- At higher Pe, induced structure from flow

Increased particle density along shoulders of particles, attempting to align in rows

Morris, J. F. “A review of microstructure in concentrated suspensions and its implications for rheology and bulk flow” (2009) 48:909-923

g(r) depends on the volume fraction

Sierou and Brady JFM (2002)

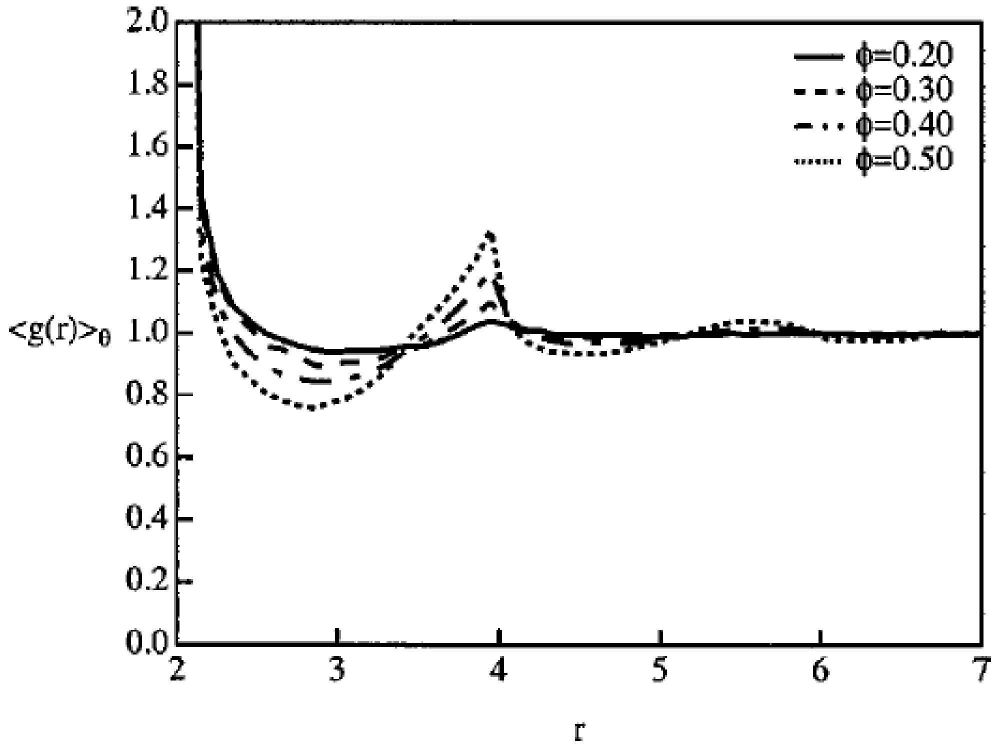

Non-Brownian

FIG. 10. The dependence of the angularly averaged pair-distribution function, $\langle g(r)\rangle_\theta$, on the volume fraction. The pair-distribution function is averaged over all orientations and results for $2 < r < 7$ are shown. Simulation results are for $N = 512$, $\tau = 1000$, and $\dot{\gamma}^\star = 1000$.

Foss and Brady JFM (2000)
Brownian hard spheres

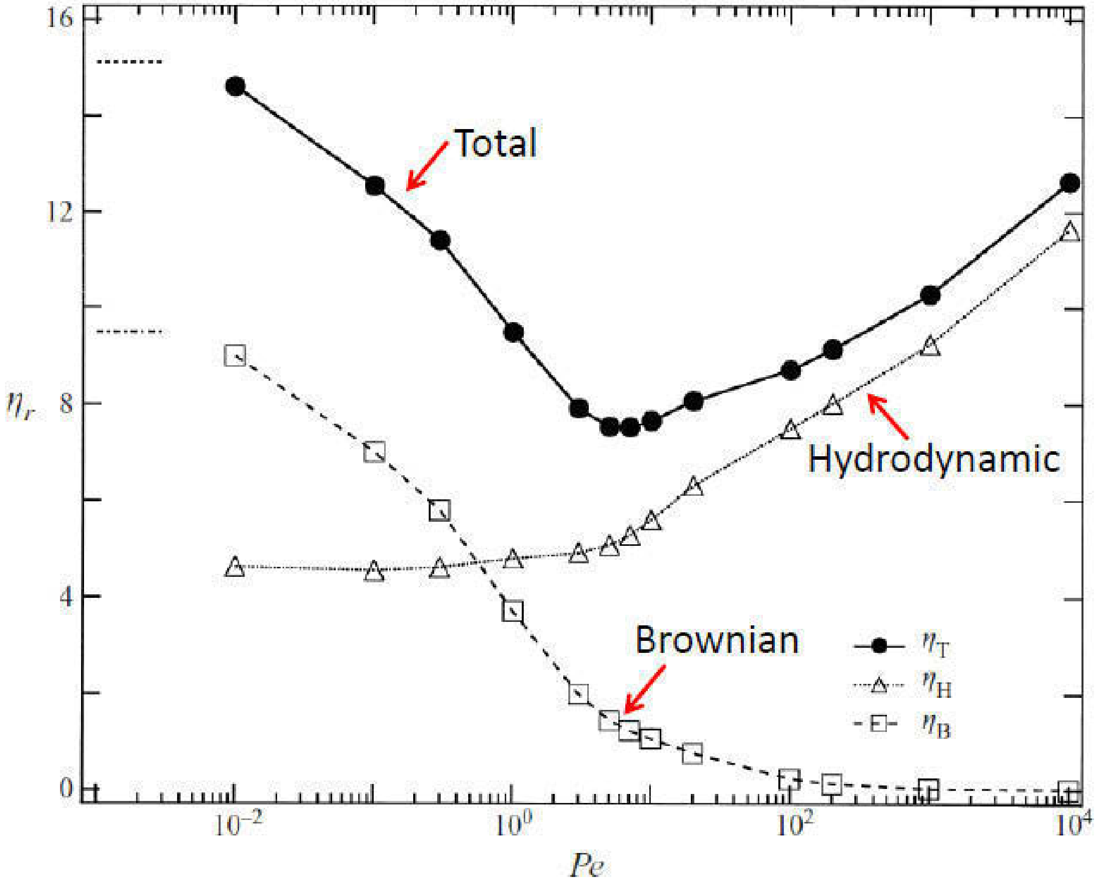

FIGURE 2. Peclet number dependence of the different contributions to the relative viscosity of hard-sphere suspensions at $\phi = 0.45$ and $N = 27$ determined by Stokesian Dynamics. The horizontal lines on the far left represent the $Pe \to 0$ limits independently determined by an equilibrium Green–Kubo analysis.

Foss and Brady JFM (2000)

Brownian hard spheres

Viscosity = f(Pe)

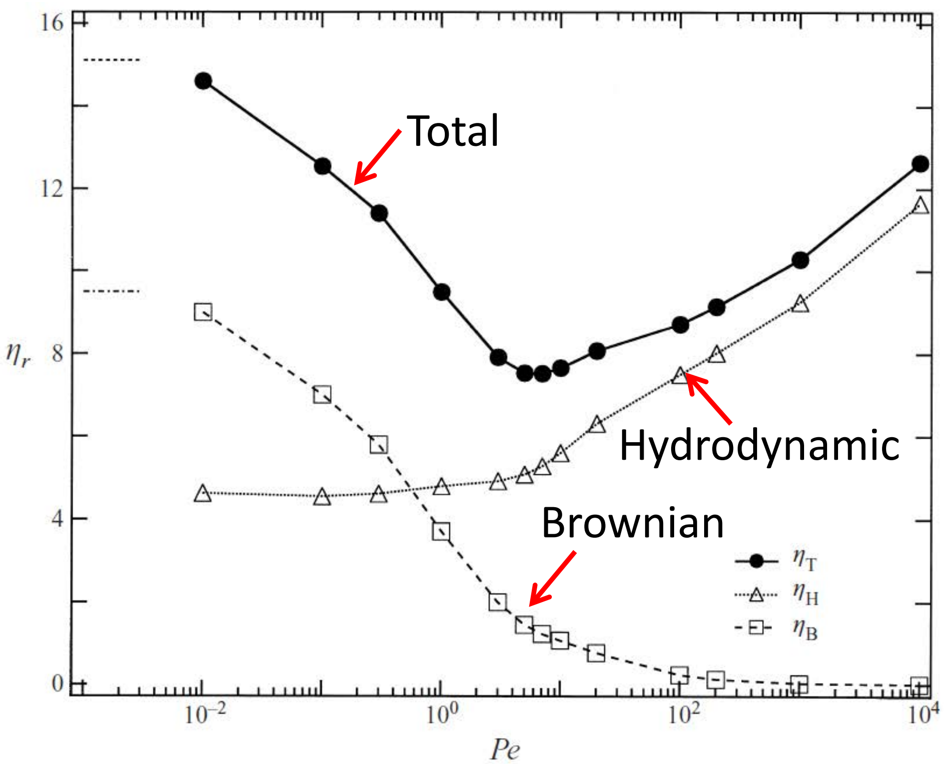

Replot as Stress = f(Pe)

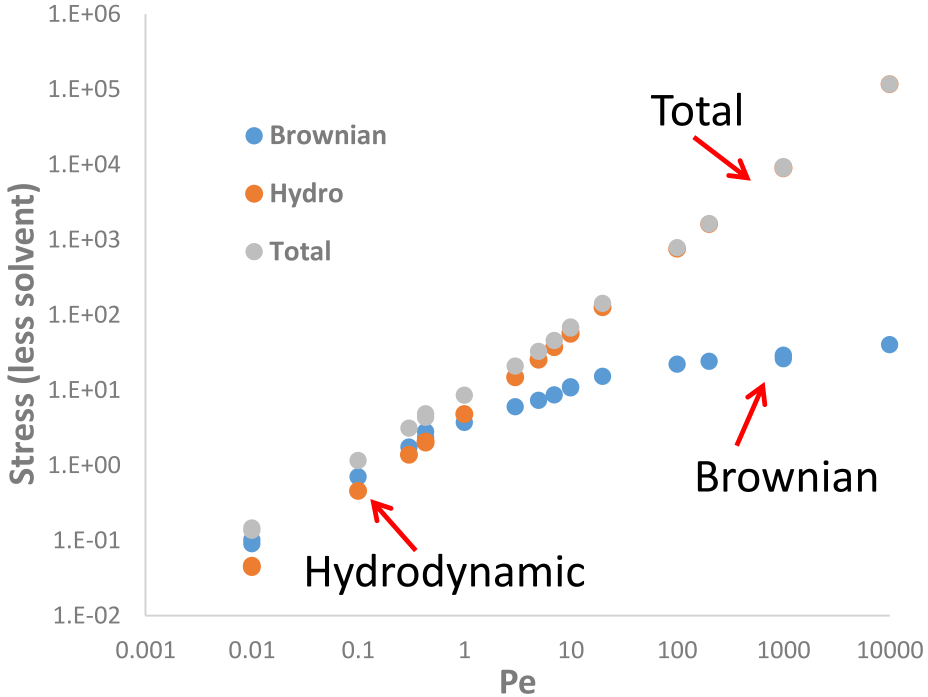

Concentrated suspensions

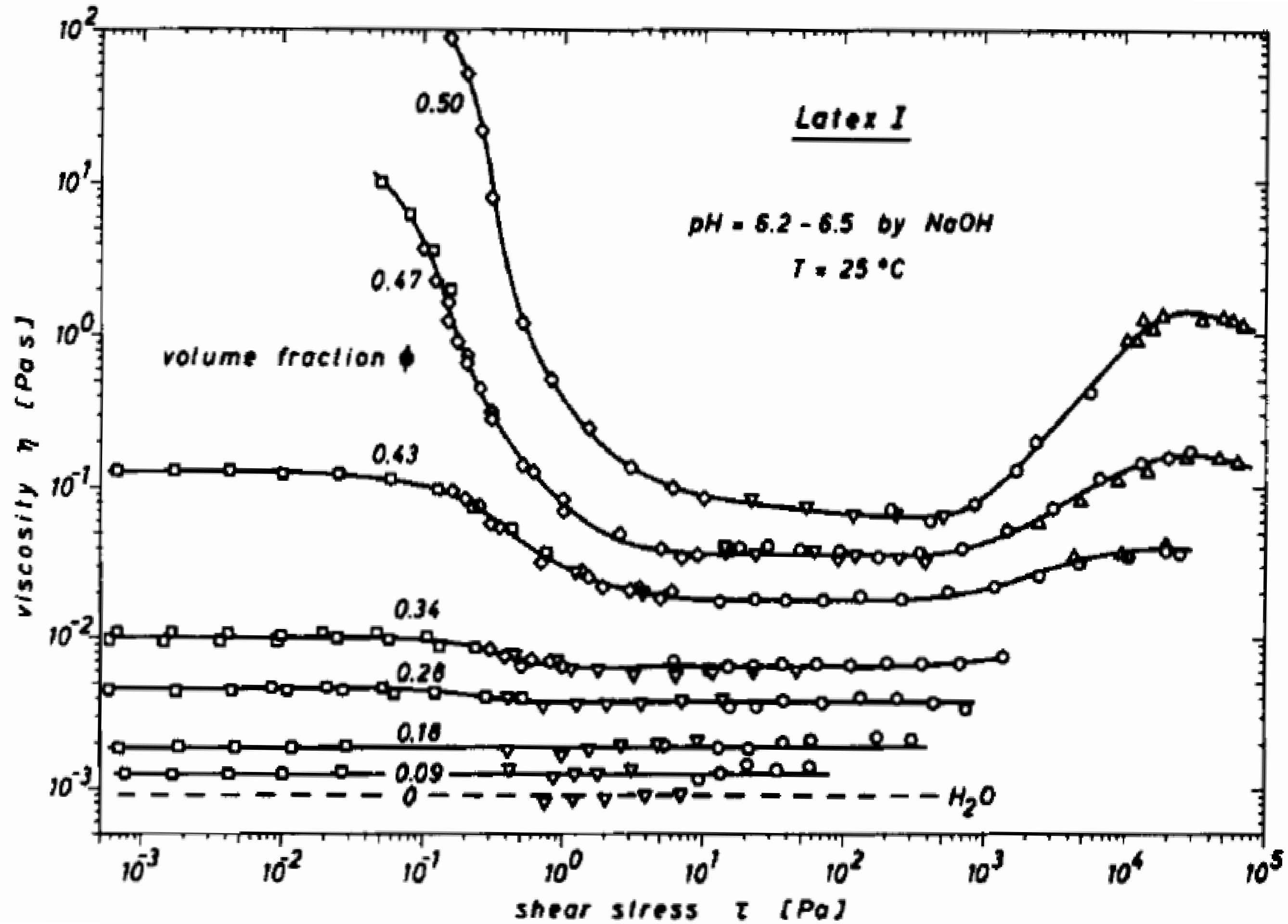

Laun, H. M. Angew. Makro. Chem. 1984, 124:335-359

Mechanisms for non-Newtonian suspension behavior

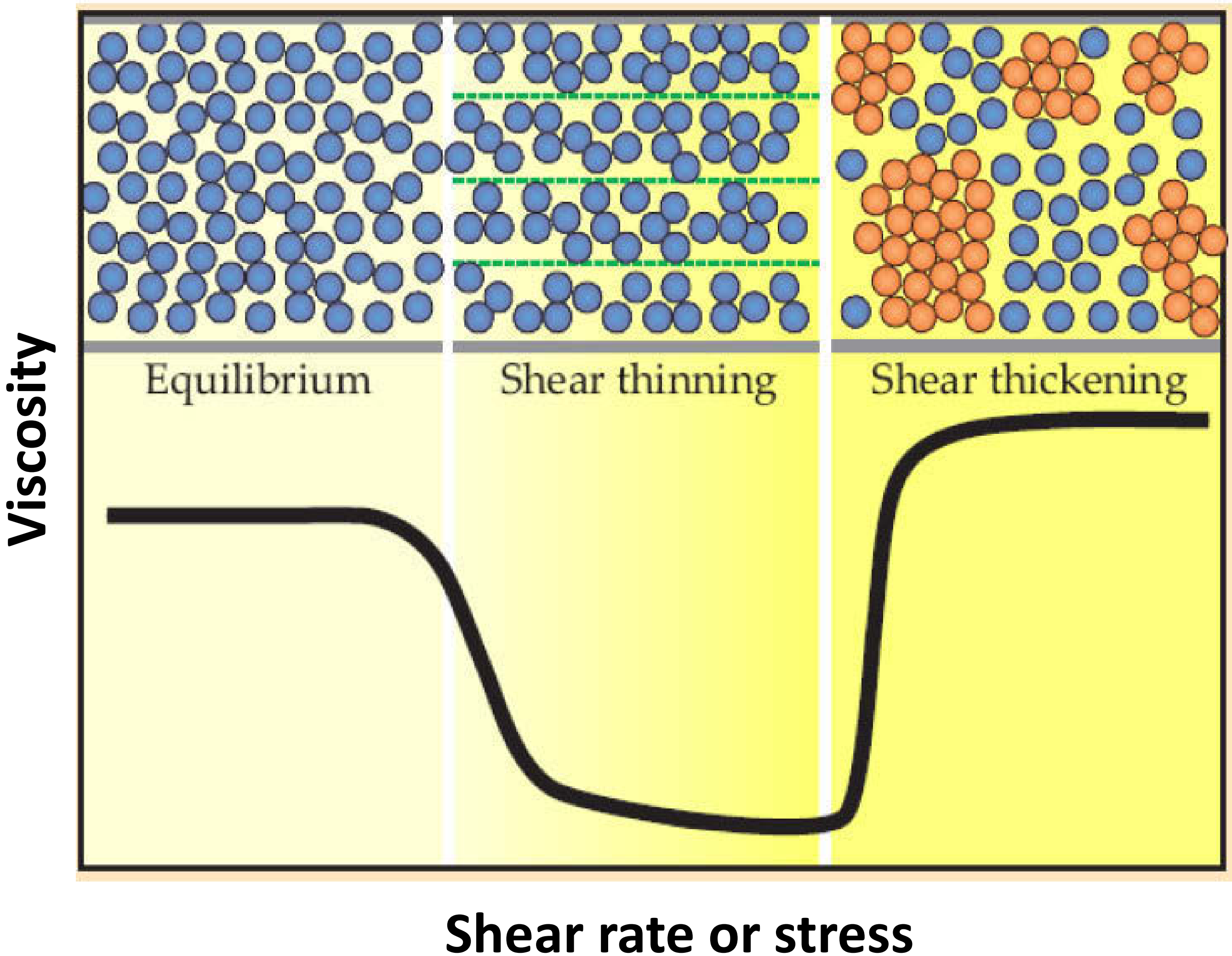

Newtonian plateau
Structure not perturbed by flow: ordering effects washed out by Brownian motion

Shear thinning
Structure is perturbed aligning particles to flow with decreased interactions

Shear thickening
Structure strongly perturbed by flow, strong rise in viscosity observed

Normal stresses in Brownian suspensions

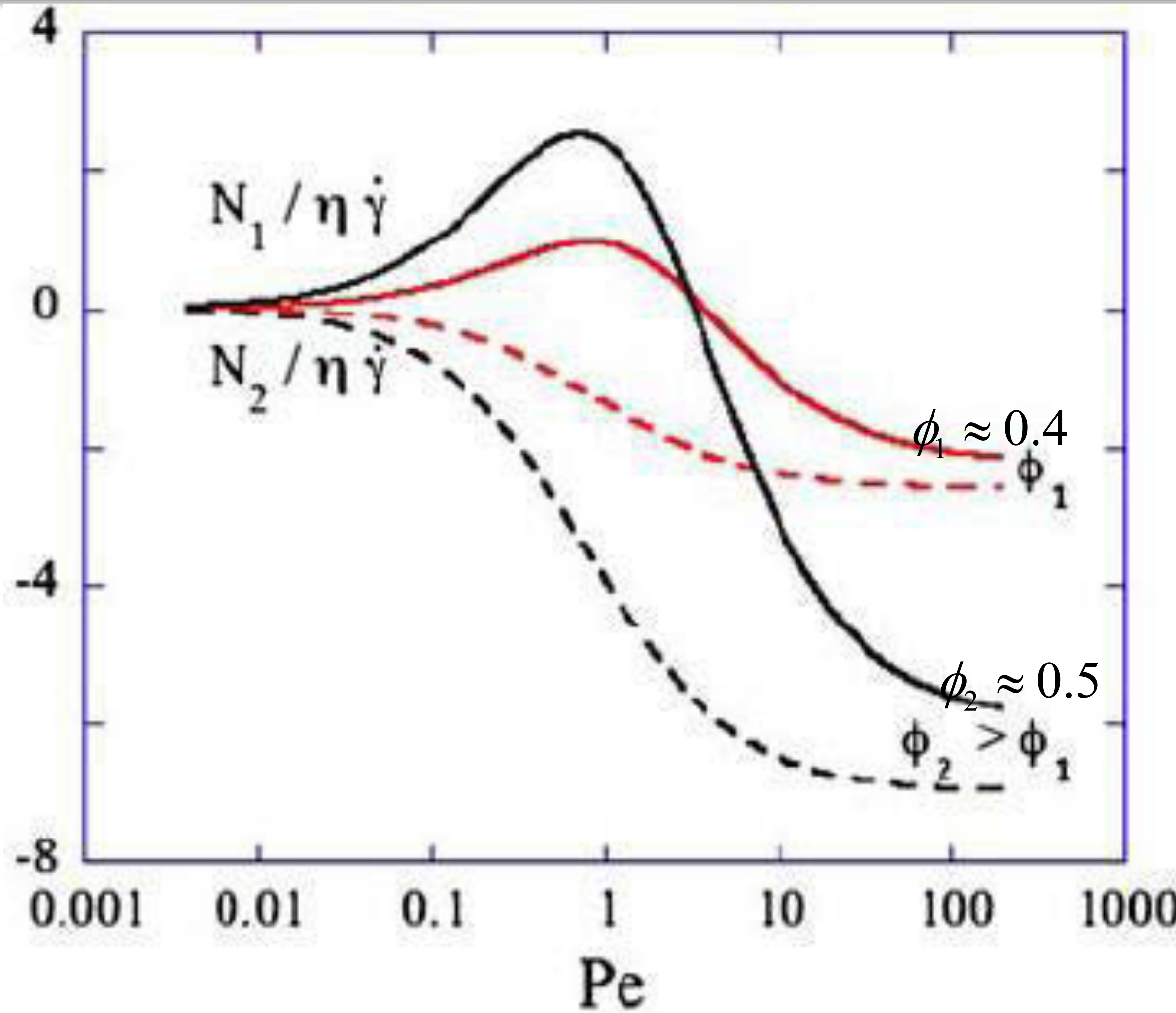

$$N_1 = \underline{\underline{\sigma}}_{11} - \underline{\underline{\sigma}}_{22}$$

(typically <0)

$$N_2 = \underline{\underline{\sigma}}_{22} - \underline{\underline{\sigma}}_{33}$$

(typically $|N_2|>|N_1|$)

Simulations

Morris, J. F. "A review of microstructure in concentrated suspensions and its implications for rheology and bulk flow" (2009) 48:909-923

Experimental agreement?

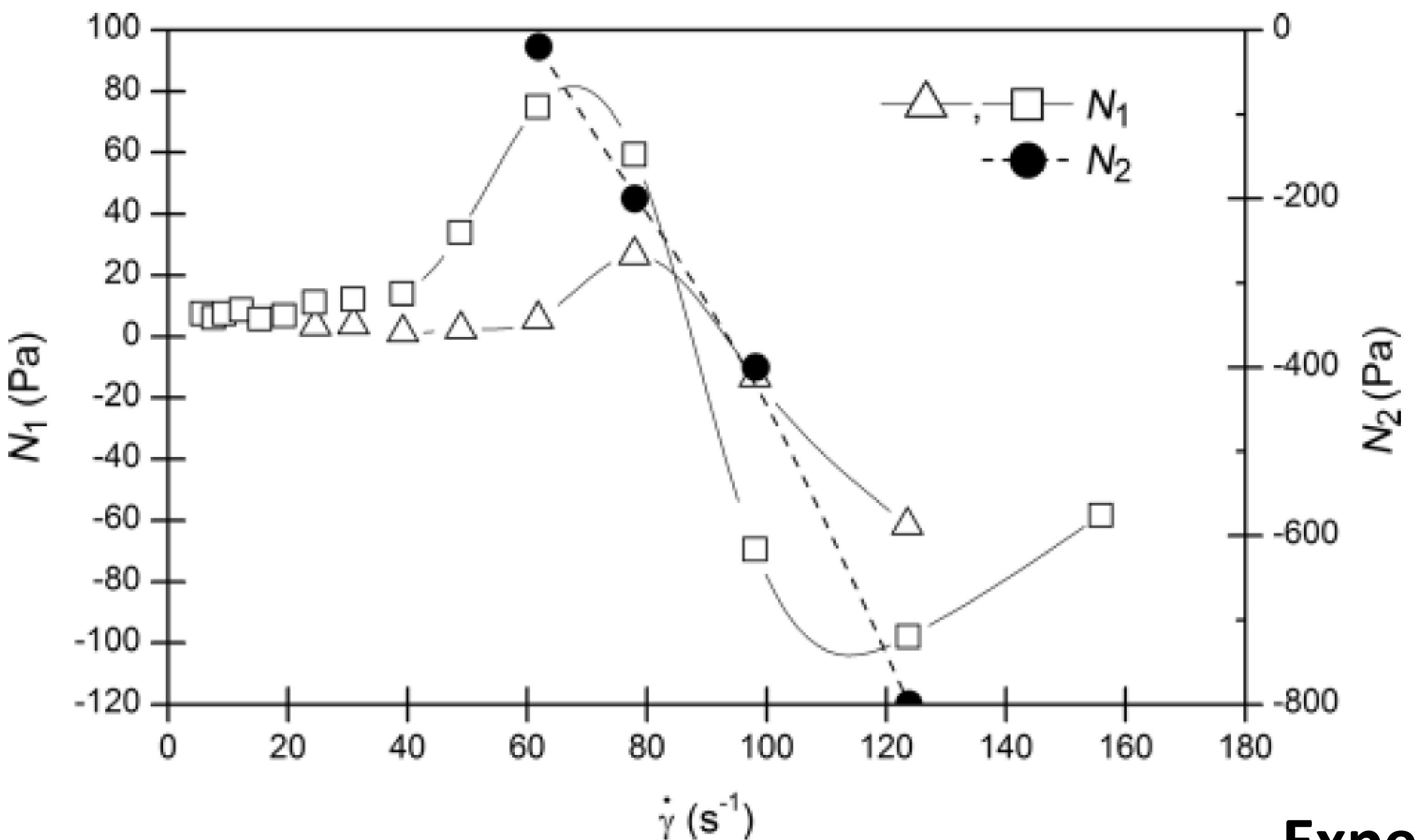

Dispersed and stabilized latex particles, 295nm radius

Experiments, Brownian

Lee, M., Alcoutlabi, M., Magda, J. J. et al. “The effect of the shear-thickening transition of model colloidal spheres on the sign of N1 and on the radial pressure profile in torsional shear flows” JoR (2006) 50:293-311

Experimental agreement?

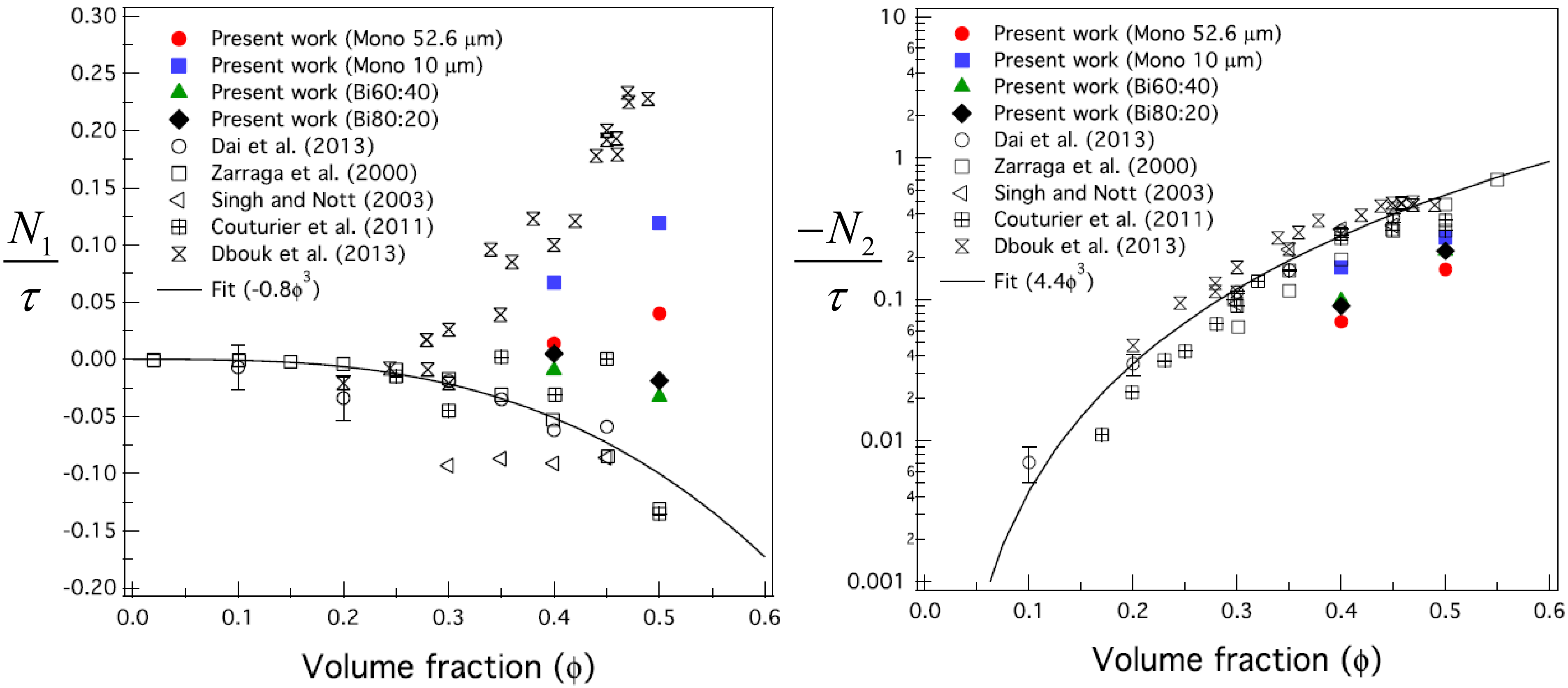

Experiments, non-Brownian

Gamonpilas, C., Morris, J. F., Denn, M. M. "Shear and normal stress measurements in non-Brownian monodisperse and bidisperse suspensions" JoR 60 (2016)

Leighton & Acrivos, JFM 1987

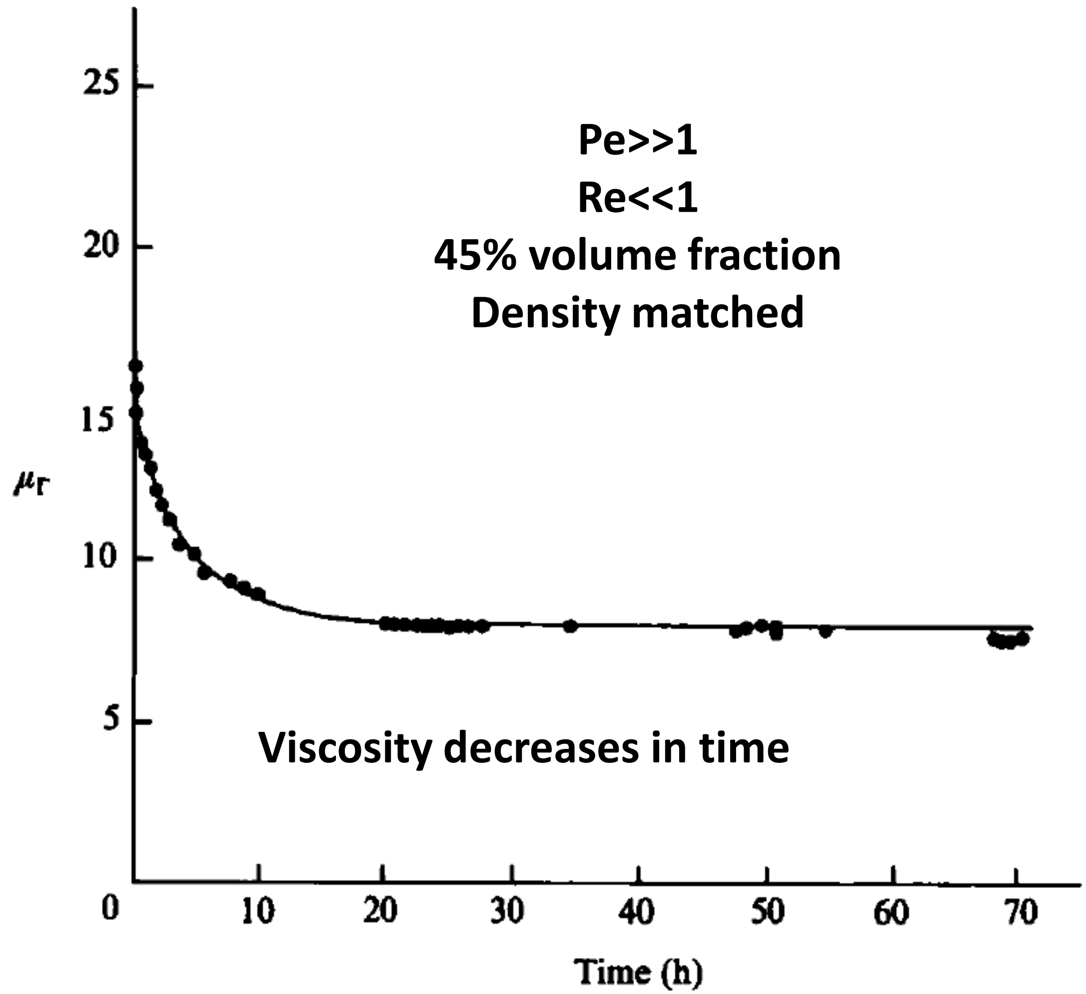

Upper geometry stationary to measure torque

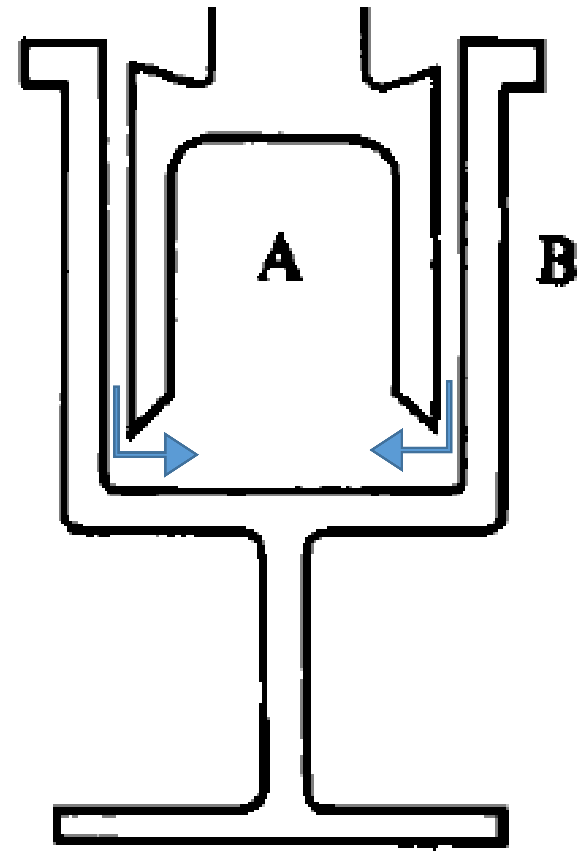

Bottom rotates

A migration model – Couette flow inside and MRI, ca. 1992

A constitutive equation for concentrated suspensions that accounts for shear-induced particle migration

Ronald J. Phillips, Robert C. Armstrong, and Robert A. Brown
Department of Chemical Engineering, Massachusetts Institute of Technology, Cambridge, Massachusetts 02139

Alan L. Graham and James R. Abbott
Los Alamos National Laboratory, Los Alamos, New Mexico 87545

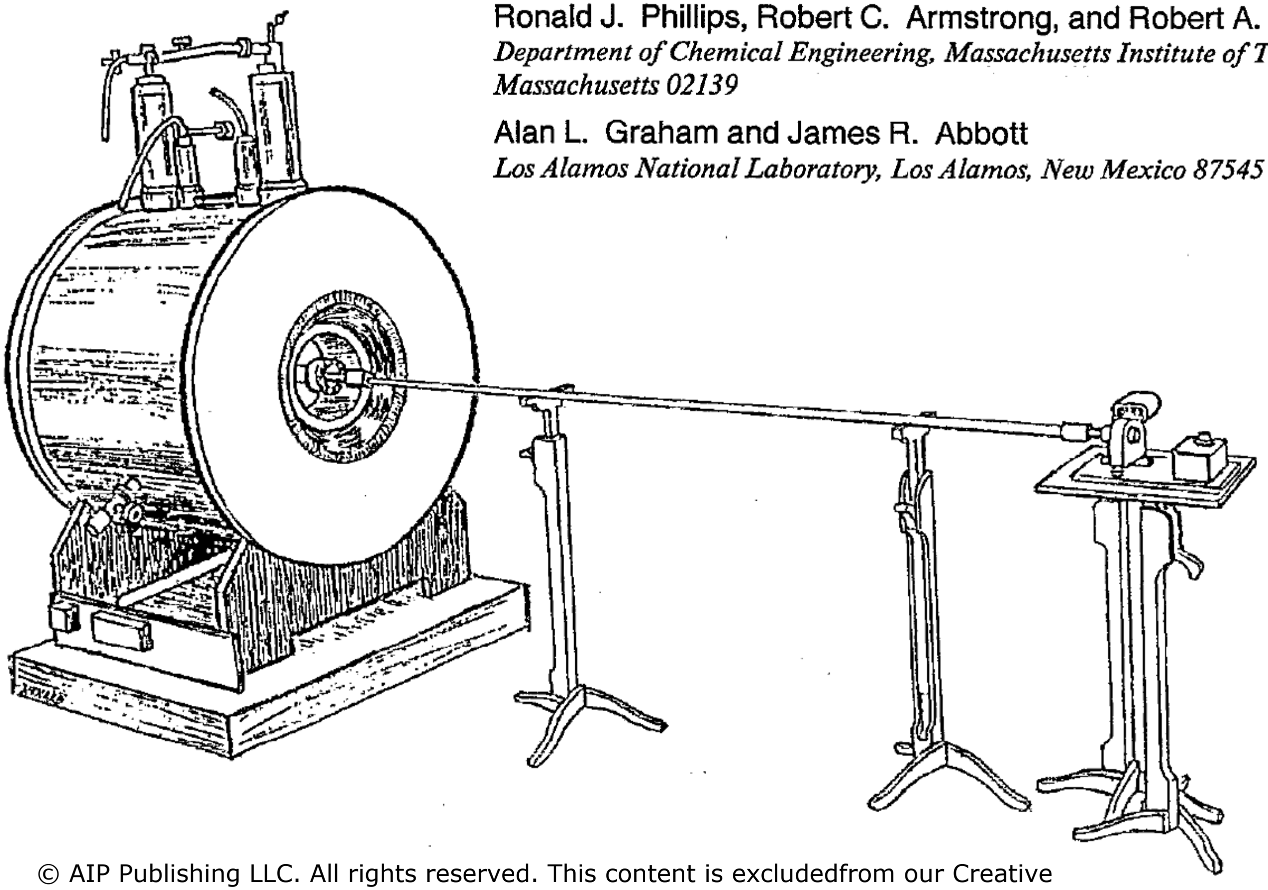

FIG. 3. Experimental NMR imaging apparatus for particle migration studies in Couette flow showing the horizontal bore magnet containing the Couette apparatus at left, the motor assembly at right, and the connecting rod.

Good agreement in steady and transient Couette flows

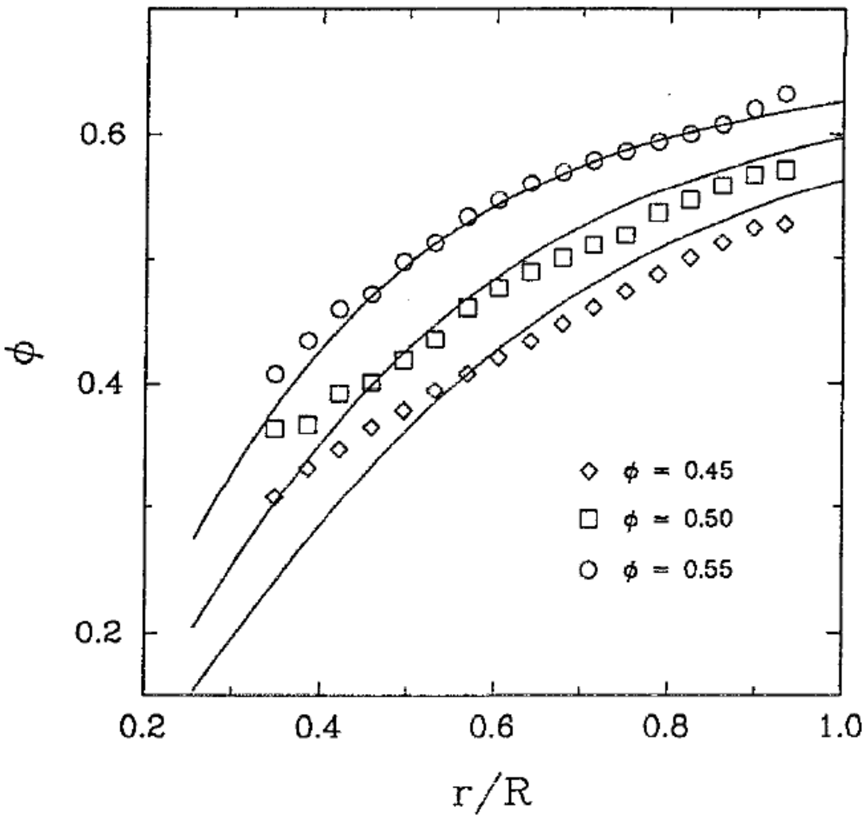

FIG. 7. Volume fraction $\phi(\hat{r})$ for three suspensions of 675 μm particles. Experimental results are for $\bar{\phi}=0.45$ (◇), $\bar{\phi}=0.50$ (□), and $\bar{\phi}=0.55$ (○) (same as in Fig. 1). Solid curves are model predictions with $K_c/K_\eta=0.66$.

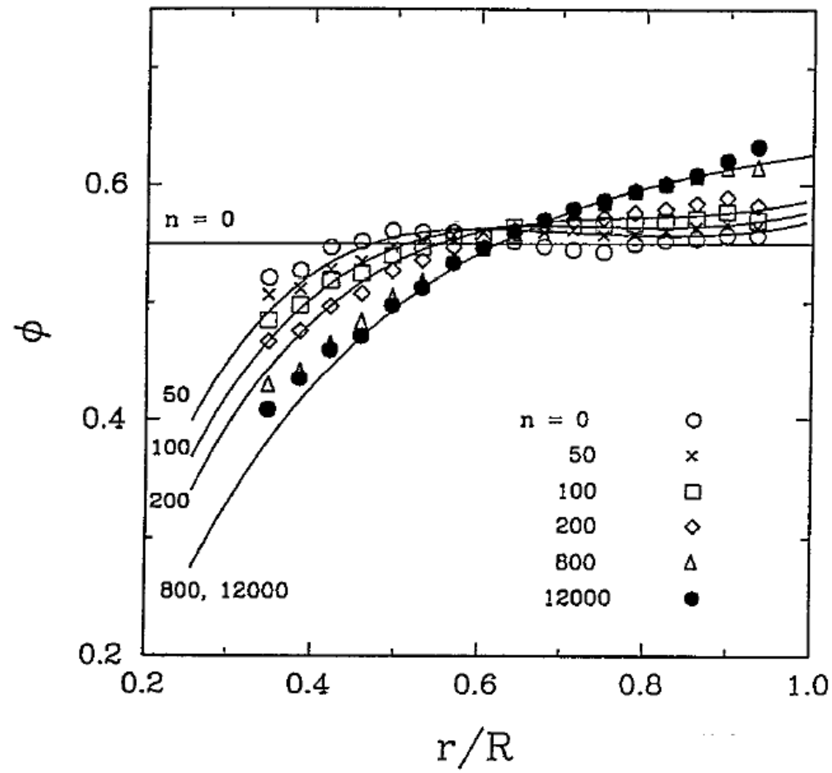

FIG. 8. Transient profiles of the particle volume fraction are shown for a suspension of 675 μm particles at $\bar{\phi}=0.55$. Results are shown for the initial profile (○) and after 50 (×), 100 (□), 200 (◇), 800 (△), and 12 000 (●) revolutions of the inner cylinder. Solid curves are the model predictions with $K_c=0.43$ and $K_\eta=0.65$.